IEEE Access
Multidisciplinary | Rapid Review | Open Access Journal

Date of publication xxxx 00, 0000, date of current version xxxx 00, 0000.

Digital Object Identifier xx.xx/ACCESS.xxxx.DOI

Secrecy Performance Analysis of Mixed $\alpha - \mu$ and Exponentiated Weibull RF-FSO Cooperative Relaying System

NAZMUL HASSAN JUEL[1,*], A. S. M. BADRUDDUZA[1,*] (Member, IEEE), S. M. RIAZUL ISLAM[2,*] (Member, IEEE), SHEIKH HABIBUL ISLAM[3], MILTON KUMAR KUNDU[4] (Member, IEEE), IMRAN SHAFIQUE ANSARI[5] (Member, IEEE), MD MUNJURE MOWLA[1], AND KYUNG-SUP KWAK[6] (Member, IEEE)

[1]Department of Electronics & Telecommunication Engineering, Rajshahi University of Engineering & Technology (RUET), Rajshahi-6204, Bangladesh (E-mail:1504038@student.ruet.ac.bd, asmb.kanon@ete.ruet.ac.bd, munjuremowla@ete.ruet.ac.bd)
[2]Department of Computer Science and Engineering, Sejong University, Seoul 05006, South Korea (E-mail: riaz@sejong.ac.kr)
[3]Department of Electrical & Electronic Engineering,RUET, Rajshahi-6204, Bangladesh (E-mail: 1501060@student.ruet.ac.bd)
[4]Department of Electrical & Computer Engineering,RUET, Rajshahi-6204, Bangladesh (E-mail: milton.kundu@ece.ruet.ac.bd)
[5]James Watt School of Engineering, University of Glasgow, Glasgow G12 8QQ, United Kingdom (E-mail: imran.ansari@glasgow.ac.uk)
[6]School of Information and Communication Engineering, Inha University, Incheon 22212, South Korea (E-mail: kskwak@inha.ac.kr)

Corresponding authors: Milton Kumar Kundu (E-mail: milton.kundu@ece.ruet.ac.bd) and Kyung-Sup Kwak (E-mail: kskwak@inha.ac.kr).
(*Nazmul Hassan Juel, A. S. M. Badrudduza, and S. M. Riazul Islam contributed equally to this work and co-first authors.)

This work was supported in part by National Research Foundation of Korea-Grant funded by the Korean Government (Ministry of Science and ICT-NRF-2020R1A2B5B02002478), and in part by Sejong university through its faculty research program (20212023).

ABSTRACT Increasing concerns regarding wireless systems' security are leading researchers to exploit the physical properties of a medium while designing any secured wireless network. The secrecy performance of a mixed radio frequency-free space optical (RF-FSO) system with a variable gain relaying scheme is investigated in this paper under the attempt of wiretapping by an eavesdropper. We assume that the eavesdropper can intrude the target data from the RF link only. Both the RF links (main and eavesdropper) undergo the $\alpha - \mu$ fading statistics and the FSO link experiences the exponentiated Weibull fading statistics. Exploiting the amplify-and-forward (AF) relaying scheme while considering two detection techniques (i.e. heterodyne detection and intensity modulation/direct detection) with pointing error impairments, the mathematical formulations of the unified probability density function and cumulative distribution function are performed for the equivalent signal-to-noise ratio of the considered dual-hop RF-FSO link. Closed-form analytical expressions for average secrecy capacity, secrecy outage probability, and the probability of non-zero secrecy capacity are derived in terms of Meijer's G and Fox's H functions to quantify the system performance. Capitalizing on these expressions, the secrecy performance is further analyzed for various channel parameters of RF links, aperture sizes of the receiver, pointing errors, and atmospheric turbulence severity. The results reveal that aperture averaging can improve the secrecy performance remarkably by suppressing the effects of turbulence. Monte Carlo simulations are provided to justify the accuracy of the proposed model.

INDEX TERMS α-μ fading, exponentiated Weibull fading, variable gain relay, physical layer security, average secrecy capacity, secrecy outage probability, probability of non-zero secrecy capacity.

I. INTRODUCTION

A. BACKGROUND

Communication is one of the most important fundamental elements for the survival of any human or organization. Researchers around the world have realized this truth and are working very hard to install a state-of-the-art communication system. Due to their efforts, the mankind is enjoying the benefits of 4G communication systems with 5G systems around the edge and already research has also begun towards the next generation / 6G communication systems. The main feature of the upcoming generation is the high-speed data-transfer to the users with maximum security. Free space

This article has been accepted for publication in a future issue of this journal, but has not been fully edited. Content may change prior to final publication. Citation information: DOI 10.1109/ACCESS.2021.3078610, IEEE Access

optical (FSO) communication is a suitable candidate for this due of its very high bandwidth, higher data rate, and sturdiness to electromagnetic interference [1]. These excellent qualities of FSO system have emerged as a well-qualified solution to the "last mile access" problem. Although FSO has some nonpareil qualities, its' sensitivity to atmospheric turbulence and unfavorable weather conditions degrades the performance and tends to reduce the data rate of this system.

B. RELATED WORKS

In recent times, significant research has been done to measure the performance of FSO communication system [1]–[13]. A survey was conducted in [1] on FSO systems with some inventive concepts such as adaptive transmission and cooperative communication diversity which deduced that FSO can be complementary to radio frequency (RF) technology. But, as mentioned earlier, there are some adverse effects that tends to minimize the performance of such system. Hence, authors in [2] presented some ways to deal with these malign issues. Spatial diversity can be one of these ways that was applied in [3], [4] to measure the average bit error rate (ABER) of exponentiated Weibull (EW) fading model. Another way to reduce the effect of atmospheric turbulence (AT) is the employment of cooperative (relay assisted) network that can significantly upgrade the performance of the FSO system by using single [5] or multiple [6] relays. This upgraded system not only can be used for general purposes but also for businesses or military applications [7].

Although, multihop communication using multiple relays presents a solution to the long distance communication problem via FSO network, the immoderate expenditure of this network makes it less feasible for practical applications. As a result, researchers started exploring some other means of long distance communications with high data rates and came up with a brilliant idea of mixed RF-FSO network that has been investigated thoroughly in [14]–[30]. In a RF-FSO network, the long distance communication takes place via the RF channel whereas the first / last mile access is provided via the FSO communication system [14]. Performance evaluation of the RF-FSO network adopting Gamma-Gamma (GG) fading model for the FSO link with various RF fading models (both multipath and generalized) have been presented in [15]–[19] where the effects of AT, pointing error (PE), and aperture size have been investigated. The advantages of having multiple antennas at the relay was also displayed in [15]. The deteriorating impact of PE and AT on generalized Gamma and Málaga fadings for FSO channels was analyzed in [20] and [21], respectively. Here, GG and Málaga fadings for FSO channel offers a good match with the experimental and simulation data for weak or strong AT. On the other hand, EW fading model shows a very tight match with both simulation and experimental data for all (weak-to-strong) turbulence conditions considering a large sized aperture in the system [6]. Because of this reason, most of the researchers have opted EW over other FSO turbulent models [22]–[26] among which the authors of [22]–[24] analyzed the impact of AT on this fading model and the impact of both AT and PE was evaluated in [25], [26]. The design and evaluation of cognitive radio RF-FSO network employing EW model was also shown in [27]. In [28], the performance of a RF-FSO network was compared with the RF-RF network, where RF-RF link exhibited slightly better performance than RF-FSO link that can be compensated by the very high data rate of the RF-FSO link. This advantage of RF-FSO network in both commercial and military communications was also confirmed by the Air Force Research Laboratory, USA [29].

In today's era, security is the most important requirement in wireless communication, especially in case of personal and military information. Hence, the RF-FSO communication systems must be secure from any eavesdropping along with it's high speed data transfer rate that has been analyzed in [31]–[36]. The secrecy outage probability (SOP) considering multiple antennas at both relay and eavesdropper, imperfect channel state information (CSI) at the RF channel, and misalignment at the GG FSO link is evaluated in [31]. Similar analysis was again performed over the same FSO link in [32] considering a simultaneous wireless information and power transfer (SWIPT) system. The impact of imperfect CSI and different relaying schemes was analyzed over the RF-FSO system with Málaga fading at the FSO link in [33], [34]. A trade-off analysis between security and reliability was also addressed in [36] considering multiuser scheduling over a Nakagami-m-GG RF-FSO model.

C. MOTIVATION AND CONTRIBUTIONS

In most of the aforementioned works, researchers have worked with GG and Málaga fading model as they can represent both weak or strong AT appropriately. But in case of aperture averaging reception, both these models fail to capture the exact practical scenario [37], [38]. This problem has been solved by introducing the EW fading model that can perfectly represent the aperture averaging at all (weak, moderate, and strong) AT conditions and this benefit of EW model has raised it's reputation among the researchers. Although some generic performance of EW has been analyzed for RF-FSO network in recent years, the security issues of this model have not been explored yet. On the other hand, $\alpha - \mu$ fading channel has some excellent qualities such as generality, flexibility, and mathematical tractability. This channel can also represent the non-linearity of the physical channel. All these positive attributes of the $\alpha-\mu$ fading channel make it a proper candidate to be utilized as RF link in the high speed RF-FSO network. Hence, in this presented work, a secure mixed RF-FSO single-input single-output (SISO) communication link is modeled with generalized $\alpha - \mu$ fading channel at the RF hop and EW fading at the FSO hop. As the narrow and highly directional beams of the FSO link make wiretapping very difficult, the eavesdropper can only interfere with the secure transmission of the RF link. The main contributions of this proposed model are:

1) At first, we present a unified probability density function (PDF) for the EW fading channel including both

detection techniques (i.e. HD and IM/DD) and pointing errors. Utilizing the PDFs and cumulative distribution function (CDF) of the respective signal-to-noise ratios (SNRs of RF and FSO links), the PDF for end-to-end SNR of dual-hop RF-FSO link is derived. To the best of authors' knowledge, the presented PDF is novel as a mixed $\alpha-\mu$ and unified EW structure is missing in the existing literature.

2) The secrecy performance of the proposed model is analyzed by evaluating novel closed-form analytical expressions for average secrecy capacity (ASC) and SOP by exploiting the Meijer's G and Fox's H functions. Subsequently, we also present a mathematical formulation of the probability of non-zero secrecy capacity (PNSC) from the expression of SOP for a particular case with zero target secrecy rate. Since, no security networks over EW channel is modeled in the previous works, the proposed model paves the way to analyze the secrecy performance when aperture averaging is considered.
3) The effect of strong-to-weak AT, pointing errors, and different fading conditions on the security of the proposed RF-FSO model is numerically analyzed and also proven through the Monte-Carlo (MC) simulations. A comparison between two detection techniques is also presented that reveals the superiority of HD technique over the IM/DD technique.

The rest of the paper is organized as follows. The proposed system RF-FSO model and the PDFs and CDFs for every individual link are presented in Section II. Section III demonstrates the derivation of closed-form expressions for ASC, SOP, and PNSC, by that order. Analytical and simulation results are exemplified in Section IV. Finally, Section V summarizes our work.

II. SYSTEM MODEL AND PROBLEM FORMULATION

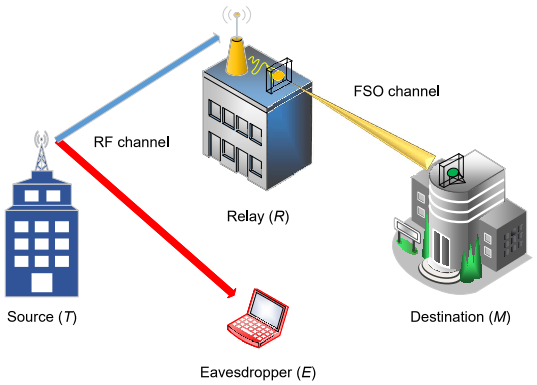

FIGURE 1: The mixed RF-FSO relaying system with source (T), relay (R), destination (M), and eavesdropper (E).

A mixed RF-FSO framework is proposed in Fig. 1, where a source, T, is transmitting a stream of secret and confidential information to the target user, M, through an intermediate relay, R, under the eavesdropper's, E, attempt to wiretap the RF link. Here, R is equipped with a single receive antenna and a single transmit photo-aperture, T and E are both furnished with a single antenna, and M houses a single receive photo-aperture. We assume that there is no direct communication link between T and M. Overall transmission takes place in two hops. Initially, T transmits information to R via the RF, $T-R$, link, R then converts the data signal to an optical signal, and finally R forwards the information to M. The $T-R$ and $T-E$ links experiences α-μ fading whereas $R-M$ link follows EW fading scenario with pointing error impairments.

The direct channel gain between T and R is defined as $g_{t,r} \in \mathbb{C}^{1\times1}$ and that between T and E is defined as $h_{t,e} \in \mathbb{C}^{1\times1}$. We denote $z \sim \widetilde{\mathcal{N}}(0, P_T)$ as the transmitted signal from T, where $\widetilde{\mathcal{N}}$ denotes a complex Gaussian distribution and P_T is the transmit power. Therefore, the received signals at R and E can be written as

$$y_R = g_{t,r}\, z + q_R, \tag{1}$$
$$y_E = h_{t,e}\, z + q_E, \tag{2}$$

where $q_R \sim \widetilde{\mathcal{N}}(0, N_R)$ and $q_E \sim \widetilde{\mathcal{N}}(0, N_E)$ are the imposed noises at R and E, respectively, considering N_R and N_E as the corresponding noise powers. Here, after receiving y_R, R converts it to optical form and then re-transmits to M via $R-M$ link with a transmit power of P_R. Therefore, received signal at M is given by

$$\begin{aligned} y_M &= h_{r,m}\, y_R + q_M \\ &= h_{r,m}\,(g_{t,r}\, z + q_R) + q_M \\ &= j_{r,m}\, z + w_M, \end{aligned} \tag{3}$$

where $h_{r,m}$ is channel gain of the link between R and M, $w_M \triangleq h_{r,m}\, q_R + q_M$, $q_M \sim \widetilde{\mathcal{N}}(0, N_M)$, N_M is the optical noise power at M, and $j_{r,m} = h_{r,m} g_{t,r}$. We can relate the electrical (P_e) and optical (P_o) powers utilizing an electrical-to-optical conversion ratio (μ) where $P_e = \mu\, P_o$.

A. PDF AND CDF OF SNR FOR THE $T-R$ LINK

The instantaneous SNR of the RF main channel can be denoted as $\gamma_m = \frac{P_T}{N_R}\|g_{t,r}\|^2$. We assume γ_m follows $\alpha-\mu$ distribution that can perfectly illustrate each phenomena due to the non-linearity of the propagation environment and clusters of multipath waves in terms of two setting parameters: α and μ. The PDF of γ_m is expressed as [39, Eq. (1)]

$$f_m(\gamma) = \mathcal{A}_1 e^{-\mathcal{A}_2\, \gamma^{\tilde{\alpha}_m}} \gamma^{\tilde{\alpha}_m \mu_m - 1}, \tag{4}$$

where $\mathcal{A}_1 = \frac{\tilde{\alpha}_m \mathcal{A}_2^{\mu_m}}{\Gamma(\mu_m)}$, $\mathcal{A}_2 = \mu_m\, \overline{\gamma}_m{}^{-\tilde{\alpha}_m}$, $\tilde{\alpha}_m = \frac{\alpha_m}{2}$, $\alpha_m > 0$ is the non-linearity parameter of the propagation environment, $\mu_m > 0$ is the number of multipath clusters, $\overline{\gamma}_m$ stands for the average SNR of the $T-R$ link with respect to which we have plotted multiple graphs in this work, and $\Gamma(\mu_m)$ designates incomplete Gamma function.

Another most important attribute of α-μ fading distribution which drives the authors to deal with this particular model is that many classical small-scale RF channels can

be obtained as special cases by exploiting different combinations of α_m and μ_m as summarized in TABLE 1. Even some large scale and composite fading models can be unified utilizing the proposed RF model [8], [39].

TABLE 1: Special cases of α-μ fading channel [39], [40].

Fading Distributions	α_m	μ_m
Rayleigh	2	1
Gamma	1	4
Nakagami-m	2	3
Weibull	3	1
Exponential	1	1

The CDF of γ_m is defined as $F_m(\gamma) = \int_0^\gamma f_m(\gamma)\, d\gamma$. Utilizing (4) and exploiting [41, Eq. (3.381.8, 8.352.6, and 8.339.1)], the CDF is expressed as

$$F_m(\gamma) = 1 - \mathcal{A}_4\, e^{-\mathcal{A}_2\, \gamma^{\tilde{\alpha}_m}}\, \gamma^{j\tilde{\alpha}_m}, \tag{5}$$

where $\mathcal{A}_4$=$\sum_{j=0}^{\mu_m-1} \frac{1}{j!}\mathcal{A}_2{}^j$.

B. PDF AND CDF OF THE SNR FOR THE EXPONENTIATED WEIBULL CHANNEL

We consider the FSO link undergoes unified EW turbulence. Considering pointing error, atmospheric path loss, and atmospheric turbulence as h_p, h_l, and h_a, respectively, the channel gain of the FSO link $h_{r,m}$ can be defined as

$$h_{r,m} = h_l h_a h_p. \tag{6}$$

Here, h_a and h_p are random terms and h_l is a deterministic term. Without any loss of generality, we assume $h_l = 1$. In the following subsections, we derive the expression of the unified EW distribution with pointing error impairments.

1) Atmospheric Turbulence Model

The PDF of h_a is given as [42, Eq. (2)]

$$f_a(h) = \frac{\alpha_o \beta_o}{\eta_o}\left(\frac{h}{\eta_o}\right)^{\beta_o-1} exp\left[-\left(\frac{h}{\eta_o}\right)^{\beta_o}\right] \times \left\{1 - exp\left[-\left(\frac{h}{\eta_o}\right)^{\beta_o}\right]\right\}^{\alpha_o-1}, \tag{7}$$

where η_0 is a scale parameter, and α_o and β_0 are shape parameters. The values of these parameters depend on the scintillation index (SI) σ_I^2, which is defined as $\sigma_I^2 = \mathbb{E}[h_a^2]/\mathbb{E}^2[h_a] - 1$ [43]. The mathematical definitions of these parameters are [44, Eq. (5)]

$$\alpha_o \simeq \frac{7.22\sigma_I^{2/3}}{\Gamma[2.487\sigma_I^{2/6} - 0.104]}, \tag{8a}$$

$$\beta_o \simeq 1.012[\alpha_o \sigma_I^2]^{-(13/25)} + 0.142, \tag{8b}$$

$$\eta_o = \frac{1}{\alpha_o \Gamma[1 + 1/\beta_o] \wedge (\alpha_o, \beta_o)}, \tag{8c}$$

$$\wedge(\alpha_o, \beta_o) = \sum_{j=0}^{\infty} \frac{(-1)^j \Gamma(\alpha_o)}{j!\Gamma(\alpha_o - j)(1+j)^{1+1/\beta_o}}. \tag{8d}$$

Note the infinite series in $\wedge(\alpha_0, \beta_0)$ converges quickly within just few terms of j (10 or less numbers of terms) and hence the numerical values of $\wedge(\alpha_0, \beta_0)$ are computed very easily. It can be pointed that for $\alpha_o = 1$, eq. (7) takes the form of Weibull fading channel. Likewise, for $\alpha_0 = 1$ and $\beta_0 = 2$, we obtain Rayleigh fading distribution and negative exponential distribution is obtained for $\alpha_0 = \beta_0 = 1$.

2) Aperture Averaging

If the irradiance correlation width is greater than the receiving aperture of the communication system, the aperture behaves as a 'point aperture'. With the increase in aperture size beyond the correlation width of the irradiance fluctuation, several correlation patches are observed at the receiver and the SI level begins decreasing, which is well-known as aperture averaging. This aperture averaging is widely used in detection system for reducing scintillation and increasing mean SNR [45]. The SI due to variation in aperture size for three optical models (i.e. Gaussian, plane, and spherical beams) are discussed below.

Gaussian Beam: According to [45], $\sigma_{I,G}^2(D)$ for a Gaussian beam propagating through a Gaussian lens (i.e. a thin lens and Gaussian limiting aperture) can be expressed as

$$\sigma_{I,G}^2(D) = \exp\left[\sigma_{\ln x,G}^2(D) + \sigma_{\ln y,G}^2(D)\right] - 1, \tag{9}$$

where $\sigma_{\ln x,G}^2(D)$ and $\sigma_{\ln y,G}^2(D)$ are the large-scale and small-scale log-irradiance flux variances that are calculated as

$$\sigma_{\ln x,G}^2(D) = \frac{0.49\left(\frac{s-\varkappa_1}{s+\varkappa_1}\right)^2 \sigma_\beta^2}{\left[0.56(1+\Lambda_1)\sigma_\beta^{\frac{12}{5}} + 0.4\,\tau_1 \sigma_\beta^{\frac{12}{7}} + 1\right]^{\frac{7}{6}}},$$

$$\sigma_{\ln y,G}^2(D) = \frac{0.51\sigma_\beta^2 / \left(0.69\,\sigma_\beta^{\frac{12}{5}} + 1\right)^{\frac{5}{6}}}{\left\{\left[1.2\left(\frac{\delta_R}{\sigma_\beta}\right)^{\frac{12}{5}} + 0.83\,\delta_R^{\frac{12}{5}}\right]/(s+\varkappa_1)\right\} + 1},$$

where $s = 4/d^2 = 16L/\left(kD^2\right) = 8\lambda L/\left(\pi D^2\right)$, Rytov variance of beam wave $\sigma_\beta^2 \cong 3.86\,\delta_R^2 \left\{0.4\left[(1+2\Lambda_1)^2 + 4\varkappa_1^2\right]^{\frac{5}{12}} \times \cos\left[\frac{5}{6}\tan^{-1}\left(\frac{1+2\Lambda_1}{2\varkappa_1}\right)\right] - \frac{11}{6}\varkappa_1^{\frac{5}{6}}\right\}$, $\tau_1 = (2-\overline{\Lambda}_1)/\left[\delta_R^{\frac{12}{7}}(s+\varkappa_1)\left(\frac{1}{3} - \frac{1}{2}\overline{\Lambda}_1 + \frac{1}{5}\overline{\Lambda}_1^2\right)^{\frac{6}{7}}\right]$, $\Lambda_1 = 1 + \frac{L_1}{F_1}$, $\overline{\Lambda}_1 = 1 - \Lambda_1$, and $\varkappa_1 = \frac{2L_1}{kW_1^2}$. Here, L_1 is the distance between input plane (transmitter) and the Gaussian lens, L_2 is the distance between the Gaussian lens and the output plane (photodetector), propagation length $L = L_1 + L_2$, $k = \frac{2\pi}{\lambda}$ is the wave number, λ is the wave length, $\delta_R^2 = 1.23\, C_n^2\, k^{7/6}\, L^{11/6}$, W_1 is the beam radius, and F_1 denotes the phase front radius of curvature at the front plane of the lens. In this particular case the coherence radius is given by $\rho_0 = \left\{8/\left[3\left(a_1 + 0.62\varkappa^{11/6}\right)\right]\right\}^{3/5}\left(1.46\, C_n^2\, k^2\, L\right)^{-3/5}$ where $a_1 = \left(1 - \Lambda^{8/3}\right)/\left(1 - \Lambda\right)$ when $\Lambda \geq 0$ and $a_1 = \left(1 + |\Lambda|^{8/3}\right)/\left(1 - \Lambda\right)$ when $\Lambda < 0$, $\Lambda = 1 + L/F$,

$\overline{\Lambda} = -L/F$, and $\varkappa = 2L/(kW^2)$. Here, F and W denote the receiver plane phase front radius of curvature and beam radius.

Plain Beam: We obtain $\sigma_{I,P}^2(D)$ considering the plane beam in the absence of inner scale and outer scale effects as [45]

$$\sigma_{I,P}^2(D) = \exp\left[\sigma_{\ln x,P}^2(D) + \sigma_{\ln y,P}^2(D)\right] - 1, \quad (10)$$

where large-scale and small-scale log-irradiance flux variances are calculated as

$$\sigma_{\ln x,P}^2(D) = \frac{0.49\,\delta_R^2}{\left(1.11\delta_R^{12/5} + 0.65s^2 + 1\right)^{7/6}}, \quad (11)$$

$$\sigma_{\ln y,P}^2(D) = \frac{0.51\delta_R^2\left(0.69\,\delta_R^{12/5} + 1\right)^{-5/6}}{0.62\,s^2\delta_R^{12/5} + 0.9\,s^2 + 1}, \quad (12)$$

where $s^2 = 2\pi D^2/(4\lambda L)$ and δ_R^2 is the Rytov variance of plane beam. The coherent radius is given by $\rho_0 = (1.46\,C_n^2\,k^2\,L)^{-3/5}$.

Spherical Beam: $\sigma_{I,S}^2(D)$ for spherical beam can be expressed as [45]

$$\sigma_{I,S}^2(D) = \exp\left[\sigma_{\ln x,S}^2(D) + \sigma_{\ln y,S}^2(D)\right] - 1, \quad (13)$$

where large-scale and small-scale log-irradiance flux variances are calculated as

$$\sigma_{\ln x,S}^2(D) = \frac{0.49\,\beta^2}{\left(0.56\,\beta^{12/5} + 0.18\,s^2 + 1\right)^{7/6}}, \quad (14)$$

$$\sigma_{\ln y,S}^2(D) = \frac{0.51\beta^2\left(0.69\,\beta^{12/5} + 1\right)^{-5/6}}{0.62\beta^{12/5}s^2 + 0.9\,s^2 + 1}, \quad (15)$$

where $\beta^2 = 0.41\delta_R^2$ is the Rytov variance of spherical wave and $s^2 = 2\pi D^2/(4\lambda L)$. In this case, the coherence radius is given by $\rho_o = (0.55\,C_n^2\,k^2\,L)^{-3/5}$.

3) Pointing Error Model

If the jitter pointing errors are taken into account, the PDF of h_p can be given as [26, Eq. (11)]

$$f_p(h) = \frac{\epsilon_o^2}{A_o{}^{\epsilon_o^2}} h^{\epsilon_o^2 - 1}, \quad (16)$$

where A_o is the fraction of the collected optical power considering the fact that there is no distance between optical spot center and the detector center, and the equivalent beamwidth is represented by $\omega_{z_{eq}}$. Moreover, $A_o = [\mathrm{erf}(\nu)]^2$ and $\omega_{z_{eq}}^2 = \omega_z^2\sqrt{\pi}\,\mathrm{erf}(\nu)/(2\,\nu\,e^{-\nu})^2$, where $\nu = \sqrt{\pi/2}\,a/\omega_z$ is the ratio between aperture radius and beam-width when the distance is z, $a = D/2$ is one half of the receiver aperture size, ω_z represents the beam waist at distance z, and erf(.) describes the error function. Further, $\epsilon_o = \omega_{z_{eq}}/(2\,\sigma_s)$ is the ratio of the equivalent beamwidth and jitter standard deviation, where σ_s denotes jitter standard deviation. In subsequent subsections, we combine atmospheric turbulence with pointing error to generate the novel composite EW PDF.

4) Composite Atmospheric Turbulence and Pointing Error Model

The PDF of composite fading $h_{r,m}$ can be determined as [26, Eq. (13)]

$$f_{r,m}(h) = \int f_{h|h_a}(h|h_a) f_{h_a}(h_a) dh_a, \quad (17)$$

where $f_{h|h_a}(h|h_a) = \frac{1}{h_l h_a} f_{h_p}\left(\frac{h}{h_l h_a}\right)$. Substituting (7) and (16) into (17) and using Newton's generalized binomial theorem $(1+z)^\rho = \sum_{j=0}^{\infty}\frac{\Gamma(\rho+1)}{j!\Gamma(\rho-j+1)}z^j$ [41, Eq. (1.110)], $f_h(h)$ is expressed as

$$f_{r,m}(h) = \frac{\alpha_o\beta_o\epsilon_o^2}{\eta_o^{\beta_o}(A_o h_l)^{\epsilon_o^2}} h^{\epsilon_o^2-1}\sum_{j=0}^{\infty}\frac{(-1)^j\Gamma(\alpha_o)}{j!\Gamma(\alpha_o - j)} \times \int_{\frac{h}{A_o h_l}}^{\infty} h_a^{\beta_o - \epsilon_o^2 - 1}\exp\left[-(1+j)\left(\frac{h_a}{\eta_o}\right)^{\beta_o}\right] dh_a. \quad (18)$$

Now, by performing random variable transformation, $y = -\beta_o \ln\frac{h}{A_o h_l h_a}$, eq. (18) takes the form as

$$f_{r,m}(h) = \frac{\alpha_o\epsilon_o^2}{(\eta_o A_o h_l)^{\beta_o}} h^{\beta_o - 1}\sum_{j=0}^{\infty}\frac{(-1)^j\Gamma(\alpha_o)}{j!\Gamma(\alpha_o - j)} \times \int_0^{\infty}\exp\left[-\frac{(1+j)h^{\beta_o}}{(\eta_o A_o h_l)^{\beta_o}}e^y - \left(\frac{\epsilon_o^2}{\beta_o} - 1\right)y\right] dy. \quad (19)$$

Utilizing [41, Eq. (3.331.2)], eq. (19) is obtained as

$$f_{r,m}(h) = \frac{\alpha_o\epsilon_o^2 h^{\epsilon_o^2-1}}{(\eta_o A_o h_l)^{\epsilon_o^2}}\sum_{j=0}^{\infty}\varrho(j)\Gamma\left(\psi, \frac{(1+j)h^{\beta_o}}{(\eta_o A_o h_l)^{\beta_o}}\right), \quad (20)$$

where $\varrho(j) = \frac{(-1)^j\Gamma(\alpha_o)}{j!\Gamma(\alpha_o - j)(1+j)^{1-\epsilon_o^2/\beta_o}}$, $\psi = 1 - \frac{\epsilon_o^2}{\beta_o}$, $\Gamma(a,x) = \int_x^{\infty} e^{-t}t^{a-1}dt$ is the upper incomplete gamma function which is defined as [41, Eq. (8.350.2)] , and h_l is assumed to be unity. Utilizing [46, Eq. (8.4.16.2)], eq. (20) is expressed as

$$f_{r,m}(h) = \frac{\alpha_o\epsilon_o^2 h^{\epsilon_o^2-1}}{(\eta_o A_o)^{\epsilon_o^2}}\sum_{j=0}^{\infty}\varrho(j)G_{1,2}^{2,0}\left[\frac{(1+j)h^{\beta_o}}{(\eta_o A_o)^{\beta_o}}\middle|\begin{matrix}1\\0,\psi\end{matrix}\right], \quad (21)$$

where $G_{c,d}^{a,b}[.]$ is Meijer's G function.

5) PDF of SNR with HD Technique

The PDF of instantaneous SNR for the FSO link utilizing HD technique is derived as

$$f_o(\gamma) = \frac{\alpha_o\,\epsilon_o^2}{\mu_h{}^{\epsilon_o^2}}\,d^{\epsilon_o^2}\,\gamma^{\epsilon_o^2-1}\sum_{j=0}^{\infty}\varrho(j) \times G_{1,2}^{2,0}\left[(1+j)d^{\beta_o}\left(\frac{\gamma}{\mu_h}\right)^{\beta_o}\middle|\begin{matrix}1\\0,\psi\end{matrix}\right], \quad (22)$$

where $d = \epsilon_o^2/\left[(1+\epsilon_o^2)\eta_o\right]$. For heterodyne detection technique, the electrical SNR $\mu_{hd} = \eta_e\mathbb{E}_h[h]/N_o = \eta_e\mathbb{E}[h_p]\mathbb{E}[h_a]/N_o = \overline{\gamma}_{o_1}$, where $\overline{\gamma}_{o_1}$ is the average SNR

This article has been accepted for publication in a future issue of this journal, but has not been fully edited. Content may change prior to final publication. Citation information: DOI 10.1109/ACCESS.2021.3078610, IEEE Access

of HD technique and $\mathbb{E}[.]$ symbolizes the expectation operator and $\mathbb{E}[h^r] = \int_0^\infty h^r f_h(h) dh$. Utilizing this equation, we obtain $\mathbb{E}[h_p] = A_o \epsilon_o^2/(1+\epsilon_o^2)$ and $\mathbb{E}[h_a] = \frac{\alpha_o}{\eta_o^{\beta_o}} \sum_{w=0}^{\infty} \binom{\alpha_o - 1}{w} (-1)^w \left(\eta_o/(1+w)\right)^{\beta_o+1}$.

Proof: See Appendix .

6) PDF of SNRs with IM/DD Technique

The PDF of instantaneous SNR for the FSO link using IM/DD technique is derived as

$$f_o(\gamma) = \frac{\alpha_o \, \epsilon_o^2}{2 \, \mu_{im}^{\frac{\epsilon_o^2}{2}}} \, d^{\epsilon_o^2} \, \gamma^{\frac{\epsilon_o^2}{2}-1} \sum_{j=0}^{\infty} \varrho(j) \times G_{1,2}^{2,0}\left[(1+j) d^{\beta_o} \left(\frac{\gamma}{\mu_{im}}\right)^{\frac{\beta_o}{2}} \middle| \begin{matrix} 1 \\ 0, \psi \end{matrix}\right], \quad (23)$$

where the electrical SNR, $\mu_{im} = \eta_e^2 \mathbb{E}_h^2[h]/N_o = \eta_e^2 \mathbb{E}_h^2[h_p] \mathbb{E}_h^2[h_a]/N_o = \overline{\gamma}_{o_2} (\epsilon_o^2+2)\epsilon_o^2/(\epsilon_o^2+1)^2/\mathbb{E}[h_a^2]$ where $\overline{\gamma}_{o_2}$ represents the average SNR of IM/DD technique and $\mathbb{E}^2[h_p] = A_o^2 \epsilon_o^4/(1+\epsilon_o^2)^2$ and $\mathbb{E}^2[h_a] = \frac{\alpha_o}{\eta_o^{\beta_o}} \sum_{w=0}^{\infty} \binom{\alpha_o - 1}{w} (-1)^w \left(\eta_o/(1+w)\right)^{\beta_o+2}$.

Proof: See Appendix .

7) Unified EW Turbulence Model with Pointing Error

The unified PDF of EW distributed atmospheric turbulent FSO link under both HD and IM/DD techniques is expressed as

$$f_o(\gamma) = \frac{\alpha_o \, \epsilon_o^2}{r \, \mu_r^{\frac{\epsilon_o^2}{r}}} \, d^{\epsilon_o^2} \, \gamma^{\frac{\epsilon_o^2}{r}-1} \sum_{j=0}^{\infty} \varrho(j) \times G_{1,2}^{2,0}\left[(1+j) d^{\beta_o} \left(\frac{\gamma}{\mu_r}\right)^{\frac{\beta_o}{r}} \middle| \begin{matrix} 1 \\ 0, \psi \end{matrix}\right], \quad (24)$$

where $r = 1$ and 2 denote the HD and IM/DD techniques, respectively and μ_r denotes electrical SNR. Utilizing [46, Eq. (2.24.2.2)], the unified CDF of instantaneous SNR is derived as

$$F_o(\gamma) = \frac{\alpha_o \, \epsilon_o^2}{\beta_o \, \mu_r^{\frac{\epsilon_o^2}{r}}} \, d^{\epsilon_o^2} \, \gamma^{\frac{\epsilon_o^2}{r}} \sum_{j=0}^{\infty} \varrho(j) \times G_{2,3}^{2,1}\left[(1+j) d^{\beta_o} \left(\frac{\gamma}{\mu_r}\right)^{\frac{\beta_o}{r}} \middle| \begin{matrix} \psi, 1 \\ 0, \psi, -\frac{\epsilon_o^2}{\beta_o} \end{matrix}\right]. \quad (25)$$

C. PDF AND CDF OF SNR FOR $T-E$ LINK

The instantaneous SNR of the $T-E$ link can be denoted as $\gamma_n = \frac{P_T}{N_E} \|h_{t,e}\|^2$. Similar to (4), the PDF of γ_n is given as [39, Eq. (1)]

$$f_n(\gamma) = \mathcal{E}_1 \, e^{-\mathcal{E}_2 \, \gamma^{\tilde{\alpha}_n}} \, \gamma^{\tilde{\alpha}_n \mu_n - 1}, \quad (26)$$

where α_n and μ_n represents the non-linearity and number of multi-path clusters of the $T-E$ link respectively, $\mathcal{E}_1 = \frac{\tilde{\alpha}_n \mathcal{E}_2^{\mu_n}}{\Gamma(\mu_n)}$, $\mathcal{E}_2 = \mu_n \, \overline{\gamma}_n{}^{-\tilde{\alpha}_n}$, $\tilde{\alpha}_n = \frac{\alpha_n}{2}$, and $\overline{\gamma}_n$ stands for the average SNR of the $T-E$ link. Similar to (5), the CDF of γ_n is expressed as

$$F_n(\gamma) = 1 - \mathcal{E}_4 \, e^{-\mathcal{E}_2 \, \gamma^{\tilde{\alpha}_n}} \, \gamma^{v \tilde{\alpha}_n}, \quad (27)$$

where $\mathcal{E}_4 = \sum_{v=0}^{\mu_n - 1} \frac{\mathcal{E}_2^v}{v!}$.

D. CDF OF SNR FOR DUAL-HOP RF-FSO LINK

The end-to-end instantaneous SNR of the variable gain relaying RF-FSO channel is given as [47, Eq. (5)]

$$\gamma_D = \frac{\gamma_o \, \gamma_m}{\gamma_o + \gamma_m + 1} \approx \min\{\gamma_o, \gamma_m\}. \quad (28)$$

The CDF of γ_D is expressed as [48]

$$F_D(\gamma_D) = 1 - \Pr[\min\{\gamma_o, \gamma_m\} \geq \gamma_D] = F_o(\gamma) + F_m(\gamma) - F_o(\gamma) \, F_m(\gamma). \quad (29)$$

Substituting (5) and (25) into (29) and exploiting some basic mathematical manipulations, the CDF of γ_D is expressed as

$$F_D(\gamma) = 1 - \sum_{j=0}^{\mu_m - 1} \mathcal{A}_4 \, e^{-\mathcal{A}_2 \, \gamma^{\tilde{\alpha}_m}} \, \gamma^{j \tilde{\alpha}_m} \times \left(1 - \frac{\alpha_o \, \epsilon_o^2}{\beta_o \, \mu_r^{\frac{\epsilon_o^2}{r}}} \, d^{\epsilon_o^2} \, \gamma^{\frac{\epsilon_o^2}{r}} \sum_{j=0}^{\infty} \varrho(j) \times G_{2,3}^{2,1}\left[(1+j) d^{\beta_o} \left(\frac{\gamma}{\mu_r}\right)^{\frac{\beta_o}{r}} \middle| \begin{matrix} \psi, 1 \\ 0, \psi, -\frac{\epsilon_o^2}{\beta_o} \end{matrix}\right]\right). \quad (30)$$

III. PERFORMANCE ANALYSIS

In this Section, we deduce the expressions of the performance metrics (i.e. ASC, SOP, and PNSC) in terms of Meijer's G and Fox's H functions. But if we consider different values of non-linearity parameters (i.e. α_m and α_n), the mathematical derivations become intractable. Hence, we consider $\alpha_m = \alpha_n$ in the later sub-sections for the ease of mathematical calculations.

A. AVERAGE SECRECY CAPACITY

ASC is the average value of the instantaneous secrecy capacity that is mathematically defined as [49, Eq. (15)]

$$\text{ASC} = \int_0^\infty \frac{1}{1+\gamma_D} \, F_n(\gamma_D) \, [1 - F_D(\gamma_D)] \, d\gamma_D. \quad (31)$$

On substituting (27) and (30) into (31), ASC is derived as

$$\text{ASC} = \mathcal{J}_1 - \mathcal{J}_2 + \mathcal{J}_3, \quad (32)$$

where $\mathcal{J}_1$, $\mathcal{J}_2$, and $\mathcal{J}_3$ are derived as follows:

1) Derivation of $\mathcal{J}_1$:

$\mathcal{J}_1$ can be written as

$$\mathcal{J}_1 = \int_0^\infty \frac{1}{1+\gamma_D} \, \mathcal{A}_4 \, e^{-\mathcal{A}_2 \, \gamma_D^{\tilde{\alpha}_m}} \, \gamma_D^{j \tilde{\alpha}_m} \, d\gamma_D. \quad (33)$$

On utilizing Meijer's G representations according to [46, Eq. (8.4.2.5 and 8.4.3.1)], $\mathcal{J}_1$ is expressed as

$$\mathcal{J}_1 = \mathcal{A}_4 \int_0^\infty \gamma_D^{j \tilde{\alpha}_m} \, G_{0,1}^{1,0}\left[\mathcal{A}_2 \, \gamma_D^{\tilde{\alpha}_m} \middle| \begin{matrix} - \\ 0 \end{matrix}\right]$$

This article has been accepted for publication in a future issue of this journal, but has not been fully edited. Content may change prior to final publication. Citation information: DOI 10.1109/ACCESS.2021.3078610, IEEE Access

$$\times G_{1,1}^{1,1}\left[\gamma_D \middle| \begin{matrix} 0 \\ 0 \end{matrix}\right] d\gamma_D. \tag{34}$$

Solving (34) with the aid of [46, Eq. (2.24.1.1)], we obtain

$$\mathcal{J}_1 = \frac{\sqrt{2}\mathcal{A}_4}{(2\pi)^{\frac{4\tilde{\alpha}_m-1}{2}}} \times G_{2\tilde{\alpha}_m,2+2\tilde{\alpha}_m}^{2+2\tilde{\alpha}_m,2\tilde{\alpha}_m}\left[\frac{\mathcal{A}_2^2}{4}\middle| \begin{matrix} \Delta(2\tilde{\alpha}_m, -j\tilde{\alpha}_m) \\ \Delta(2,0), \Delta(2\tilde{\alpha}_m, -j\tilde{\alpha}_m) \end{matrix}\right], \tag{35}$$

where $\Delta(m,a) = \{\frac{a}{m}, \frac{a+1}{m}, ..., \frac{a+m-1}{m}\}$.

2) Derivation of $\mathcal{J}_2$:

$\mathcal{J}_2$ is expressed as

$$\mathcal{J}_2 = \int_0^\infty \frac{\mathcal{A}_4\,\mathcal{E}_4}{1+\gamma_D} e^{-\gamma_D^{\tilde{\alpha}_m(\mathcal{A}_2+\mathcal{E}_2)}} \gamma_D^{(j+v)\tilde{\alpha}_m} d\gamma_D. \tag{36}$$

On utilizing Meijer's G function representations according to [46, Eq. (8.4.2.5 and 8.4.3.1)], $\mathcal{J}_2$ is expressed as

$$\mathcal{J}_2 = \mathcal{A}_4\,\mathcal{E}_4 \int_0^\infty \gamma_D^{(j+v)\tilde{\alpha}_m} \times G_{0,1}^{1,0}\left[(\mathcal{A}_2+\mathcal{E}_2)\,\gamma_D^{\tilde{\alpha}_m}\middle| \begin{matrix} - \\ 0 \end{matrix}\right] G_{1,1}^{1,1}\left[\gamma_D\middle| \begin{matrix} 0 \\ 0 \end{matrix}\right], \tag{37}$$

which is solved, similar to (35), as

$$\mathcal{J}_2 = \frac{\sqrt{2}\,\mathcal{A}_4\mathcal{E}_4}{(2\pi)^{\frac{2\alpha_m-1}{2}}} \times G_{\alpha_m,2+\alpha_m}^{2+\alpha_m,\alpha_m}\left[\frac{(\mathcal{A}_2+\mathcal{E}_2)^2}{4}\middle| \begin{matrix} \Delta(\alpha_m, \mathcal{S}) \\ \Delta(2,0), \Delta(\alpha_m, \mathcal{S}) \end{matrix}\right], \tag{38}$$

where $\mathcal{S}$=$-(j+v)\,\tilde{\alpha}_m$.

3) Derivation of $\mathcal{J}_3$:

$\mathcal{J}_3$ is expressed as

$$\mathcal{J}_3 = \int_0^\infty \frac{\mathcal{A}_4\,\mathcal{E}_4\,\mathcal{X}_1}{1+\gamma_D} e^{-\gamma_D^{\tilde{\alpha}_m(\mathcal{A}_2+\mathcal{E}_2)}} \gamma_D^{\mathcal{Y}_1-1} \times G_{2,3}^{2,1}\left[\mathcal{X}_2\gamma_D^{\frac{\beta_o}{r}}\middle| \begin{matrix} \psi, 1 \\ 0, \psi, -\frac{\epsilon_o^2}{\beta_o} \end{matrix}\right] d\gamma_D, \tag{39}$$

where $\mathcal{X}_1$=$\frac{\alpha_o\,\epsilon_o^2 d^{\epsilon_o^2}}{\beta_o\,\mu_r^{\frac{\epsilon_o^2}{r}}} \sum_{j=0}^\infty \varrho(j)$, $\mathcal{Y}_1$=$(j+v)\tilde{\alpha}_m + \frac{\epsilon_o^2}{r} + 1$, and $\mathcal{X}_2$=$\frac{(1+j)d_o^\beta}{\mu_r^{\frac{\beta_o}{r}}}$. On utilizing Meijer's G function representations according to [46, Eq. (8.4.2.5 and 8.4.3.1)], $\mathcal{J}_3$ is expressed as

$$\mathcal{J}_3 = \mathcal{A}_4\,\mathcal{E}_4\,\mathcal{X}_1 \int_0^\infty \gamma_D^{\mathcal{Y}_1-1} G_{0,1}^{1,0}\left[(\mathcal{A}_2+\mathcal{E}_2)\,\gamma_D^{\tilde{\alpha}_m}\middle| \begin{matrix} - \\ 0 \end{matrix}\right] \times G_{1,1}^{1,1}\left[\gamma_D\middle| \begin{matrix} 0 \\ 0 \end{matrix}\right] G_{2,3}^{2,1}\left[\mathcal{X}_2\gamma_D^{\frac{\beta_o}{r}}\middle| \begin{matrix} \psi, 1 \\ 0, \psi, -\frac{\epsilon_o^2}{\beta_o} \end{matrix}\right] d\gamma_D. \tag{40}$$

$$\mathcal{J}_3 = \frac{\mathcal{A}_4\,\mathcal{E}_4\,\mathcal{X}_1}{\tilde{\alpha}_m} \int_0^\infty x^{\frac{\mathcal{Y}_1}{\tilde{\alpha}_m}-1} G_{0,1}^{1,0}\left[(\mathcal{A}_2+\mathcal{E}_2)\,x\middle| \begin{matrix} - \\ 0 \end{matrix}\right] \times G_{1,1}^{1,1}\left[x^{\frac{1}{\tilde{\alpha}_m}}\middle| \begin{matrix} 0 \\ 0 \end{matrix}\right] G_{2,3}^{2,1}\left[\mathcal{X}_2 x^{\frac{\beta_o}{\tilde{\alpha}_m r}}\middle| \begin{matrix} \psi, 1 \\ 0, \psi, -\frac{\epsilon_o^2}{\beta_o} \end{matrix}\right] dx. \tag{41}$$

Note that, the integration operation in (41) includes three Meijer's G functions, which is mathematically difficult to solve. To accomplish this task, we extend the Meijer's G function to Fox's H function according to [50, Eq. (6.2.8)] and obtain

$$\mathcal{J}_3 = \frac{\mathcal{A}_4\,\mathcal{E}_4\,\mathcal{X}_1}{\tilde{\alpha}_m} \int_0^\infty x^{\frac{\mathcal{Y}_1}{\tilde{\alpha}_m}-1} H_{0,1}^{1,0}\left[(\mathcal{A}_2+\mathcal{E}_2)\,x\middle| \begin{matrix} - \\ (0,1) \end{matrix}\right] \times H_{1,1}^{1,1}\left[x^{\frac{1}{\tilde{\alpha}_m}}\middle| \begin{matrix} (0,1) \\ (0,1) \end{matrix}\right] \times H_{2,3}^{2,1}\left[\mathcal{X}_2 x^{\frac{\beta_o}{\tilde{\alpha}_m r}}\middle| \begin{matrix} (\psi,1),(1,1) \\ (0,1),(\psi,1),(-\frac{\epsilon_o^2}{\beta_o},1) \end{matrix}\right] dx. \tag{42}$$

We solve (42) utilizing [51, Eq. (2.3)] and further simplify utilizing [39, Eq. (3)] as shown in (43).

B. SECRECY OUTAGE PROBABILITY

A perfect secrecy can only be achieved when the instantaneous secrecy capacity, C_s, is greater than a predefined target secrecy rate, R_s, i.e. $R_s \leqslant C_s$. When C_s falls below R_s, an outage occurs. The SOP of a mixed RF-FSO system in the presence of an eavesdropper can be defined as [52, Eq. (14)]

$$\begin{aligned} \text{SOP} &= Pr\left\{C_s(\gamma_D, \gamma_n) \leqslant R_s\right\} \\ &= Pr\left\{\gamma_D \leqslant \Theta(\gamma_n+1) - 1\right\} \\ &= \int_0^\infty F_D\left(\Theta\,\gamma_n + \Theta - 1\right) f_n\left(\gamma_n\right) d\gamma_n, \end{aligned} \tag{44}$$

where $\Theta = 2^{R_s}$ and $R_s > 0$. Substituting (26) and (30) into (44), the SOP is expressed as

$$\text{SOP} = 1 - \mathcal{K}_1 + \mathcal{K}_2, \tag{45}$$

where $\mathcal{K}_1$ and $\mathcal{K}_2$ are derived as follows:

1) Derivation of $\mathcal{K}_1$:

$\mathcal{K}_1$ is written as

$$\mathcal{K}_1 = \int_0^\infty \mathcal{A}_4\mathcal{E}_1\, e^{-\mathcal{A}_2\,(\Theta\gamma+\Theta-1)^{\tilde{\alpha}_m}} e^{-\mathcal{E}_2\gamma^{\tilde{\alpha}_n}}$$

$$\mathcal{J}_3 = \frac{\mathcal{A}_4\,\mathcal{E}_4\,\mathcal{X}_1\,(\mathcal{A}_2+\mathcal{E}_2)^{-\frac{\mathcal{Y}_1}{\tilde{\alpha}_m}}}{\tilde{\alpha}_m} \times H_{1,0;1,1;2,3}^{1,0;1,1;2,1}\left[\begin{matrix} 1-\frac{\mathcal{Y}_1}{\tilde{\alpha}_m}; \frac{1}{\tilde{\alpha}_m}; \frac{\beta_o}{\tilde{\alpha}_m r} \\ - \end{matrix}\middle| \begin{matrix} (0,1) \\ (0,1) \end{matrix}\middle| \begin{matrix} (\psi,1),(1,1) \\ (0,1),(\psi,1),(-\frac{\epsilon_o^2}{\beta_o},1) \end{matrix}\middle| (\mathcal{A}_2+\mathcal{E}_2)^{-\frac{1}{\tilde{\alpha}_m}}, \frac{\mathcal{X}_2}{(\mathcal{A}_2+\mathcal{E}_2)^{\frac{\beta_o}{\tilde{\alpha}_m r}}}\right]. \tag{43}$$

$$\times (\Theta\gamma + \Theta - 1)^{j\tilde{\alpha}_m} \gamma^{\tilde{\alpha}_n \mu_n - 1} d\gamma. \tag{46}$$

Exploiting [41, Eq. (1.111)], eq. (46) is simplified as

$$\mathcal{K}_1 = \sum_{n_1=0}^{j\tilde{\alpha}_m} \mathcal{A}_5 \mathcal{E}_1 \mathcal{A}_4 \mathcal{F}_1 \int_0^{\infty} e^{-(\mathcal{A}_3 + \mathcal{E}_2)\gamma^{\tilde{\alpha}_m}} \gamma^{\tilde{\alpha}_n \mu_n + n_1 - 1} d\gamma, \tag{47}$$

where $\mathcal{F}_1 = \binom{j\tilde{\alpha}_m}{n_1} (\Theta - 1)^{j\tilde{\alpha}_m - n_1} \Theta^{n_1}$, $\mathcal{A}_5 = e^{-\mathcal{A}_2 (\Theta - 1)^{\tilde{\alpha}_m}}$, and $\mathcal{A}_3 = \mathcal{A}_2 \Theta^{\tilde{\alpha}_m}$. Eq. (47) is solved utilizing [41, Eq. (3.381.10)] as

$$\mathcal{K}_1 = \sum_{n_1=0}^{j\tilde{\alpha}_m} \frac{\mathcal{A}_5 \mathcal{E}_1 \mathcal{A}_4 \mathcal{F}_1}{(\mathcal{A}_3 + \mathcal{E}_2)^{\frac{\tilde{\alpha}_n \mu_n + n_1}{\tilde{\alpha}_m}} \tilde{\alpha}_m} \left(\frac{\tilde{\alpha}_n \mu_n + n_1}{\tilde{\alpha}_m} - 1 \right)!. \tag{48}$$

2) Derivation of $\mathcal{K}_2$

$\mathcal{K}_2$ is expressed as

$$\mathcal{K}_2 = \int_0^{\infty} \mathcal{E}_1 \mathcal{A}_4 \mathcal{X}_1 e^{-\mathcal{A}_2 (\Theta\gamma + \Theta - 1)^{\tilde{\alpha}_m}} e^{-\mathcal{E}_2 \gamma^{\tilde{\alpha}_n}} \times (\Theta\gamma + \Theta - 1)^{j\tilde{\alpha}_m + \frac{\epsilon_o^2}{r}} \gamma^{\tilde{\alpha}_n \mu_n - 1} \times G_{2,3}^{2,1} \left[\mathcal{X}_2 (\Theta\gamma + \Theta - 1)^{\frac{\beta_o}{r}} \middle| \begin{matrix} \psi, 1 \\ 0, \psi, -\frac{\epsilon_o^2}{\beta_o} \end{matrix} \right] d\gamma. \tag{49}$$

Utilizing the binomial theorem of [41, Eqs. (1.110 and 1.111)], (49) is simplified to

$$\mathcal{K}_2 = \sum_{n_2=0}^{\infty} \sum_{k_1=0}^{n_2} \sum_{n_3=0}^{\infty} \sum_{k_2=0}^{n_3} \int_0^{\infty} \mathcal{E}_1 \mathcal{A}_4 \mathcal{X}_1 \mathcal{A}_5 \mathcal{F}_2 \gamma^{\tilde{\alpha}_n \mu_n + k_1 - 1} \times e^{-(\mathcal{A}_3 + \mathcal{E}_2)\gamma^{\tilde{\alpha}_m}} G_{2,3}^{2,1} \left[\mathcal{X}_2 \mathcal{F}_3 \gamma^{k_2} \middle| \begin{matrix} \psi, 1 \\ 0, \psi, -\frac{\epsilon_o^2}{\beta_o} \end{matrix} \right] d\gamma, \tag{50}$$

where $\mathcal{F}_2 = (-1)^{j\tilde{\alpha}_m + \epsilon_o^2/r + n_2} \binom{j\tilde{\alpha}_m + \epsilon_o^2/r}{n_2} \Theta^{n_2} \binom{n_2}{k_1}$ and $\mathcal{F}_3 = (-1)^{\beta_o/r + n_3} \binom{\beta_o/r}{n_3} \Theta^{n_3} \binom{n_3}{k_2}$. Now, on utilizing Meijer's G function representations according to [46, Eq. (8.4.3.1)], $\mathcal{K}_2$ is expressed as

$$\mathcal{K}_2 = \sum_{n_2=0}^{\infty} \sum_{k_1=0}^{n_2} \sum_{n_3=0}^{\infty} \sum_{k_2=0}^{n_3} \int_0^{\infty} \mathcal{E}_1 \mathcal{A}_4 \mathcal{X}_1 \mathcal{A}_5 \mathcal{F}_2 \gamma^{\tilde{\alpha}_n \mu_n + k_1 - 1} \times G_{0,1}^{1,0} \left[(\mathcal{A}_3 + \mathcal{E}_2) \gamma_D^{\tilde{\alpha}_m} \middle| \begin{matrix} - \\ 0 \end{matrix} \right] \times G_{2,3}^{2,1} \left[\mathcal{X}_2 \mathcal{F}_3 \gamma^{k_2} \middle| \begin{matrix} \psi, 1 \\ 0, \psi, -\frac{\epsilon_o^2}{\beta_o} \end{matrix} \right] d\gamma. \tag{51}$$

Now, letting $x = \gamma^{\tilde{\alpha}_m}$ in (51), we have

$$\mathcal{K}_2 = \sum_{n_2=0}^{\infty} \sum_{k_1=0}^{n_2} \sum_{n_3=0}^{\infty} \sum_{k_2=0}^{n_3} \frac{\mathcal{E}_1 \mathcal{A}_4 \mathcal{X}_1 \mathcal{A}_5 \mathcal{F}_2}{\tilde{\alpha}_m} \times \int_0^{\infty} x^{\frac{\tilde{\alpha}_n \mu_n + k_1}{\tilde{\alpha}_m} - 1} G_{0,1}^{1,0} \left[(\mathcal{A}_3 + \mathcal{E}_2) x \middle| \begin{matrix} - \\ 0 \end{matrix} \right] \times G_{2,3}^{2,1} \left[\mathcal{X}_2 \mathcal{F}_3 x^{\frac{k_2}{\tilde{\alpha}_m}} \middle| \begin{matrix} \psi, 1 \\ 0, \psi, -\frac{\epsilon_o^2}{\beta_o} \end{matrix} \right] dx. \tag{52}$$

We solve (52) by utilizing [46, Eq. (2.24.1.1)] and obtain the final result as expressed in (53).

C. PROBABILITY OF NON-ZERO SECRECY CAPACITY

C_s must be positive to ensure a secure communication otherwise, the transmitted data will be vulnerable to wiretapping. In this respect, PNSC is a fundamental benchmark for secrecy analysis that can be expressed as [53]

$$\begin{aligned} \text{PNSC} &= Pr(C_s > 0) \\ &= 1 - \text{SOP}|_{R_s = 0}. \end{aligned} \tag{54}$$

Applying $R_s = 0$ in (45), the PNSC is derived as shown in (55).

D. GENERALITY OF ASC, SOP, AND PNSC EXPRESSIONS

In order to design a perfectly secure RF-FSO framework, we derive the expressions for secrecy performance metrics such as ASC, SOP, & PNSC with respect to the fading parameters of both RF and FSO hops. Based on aforementioned literature, to the best of the authors' knowledge, our derived expressions in (32), (45), & (55), respectively, are novel. For a special case of $\alpha_o = 1$, the PDF of EW distribution reduces to the PDF of Weibull distribution [54, Eq. (8)]. Furthermore, the PDF of Weibull distribution can be reduced to the PDFs of negative exponential and Rayleigh for cases when $\beta_o = 1$ & $\beta_o = 2$, respectively, as mentioned in [54].

IV. NUMERICAL RESULTS

We utilize the expressions in (32), (45), and (55) to present some numerical examples with figures for better understanding of each system parameter (i.e. atmospheric turbulence, fading, pointing errors, detection techniques, etc.) on the secrecy performance. At the same time, in each figure, a set

$$\mathcal{K}_2 = \sum_{n_2=0}^{\infty} \sum_{k_1=0}^{n_2} \sum_{n_3=0}^{\infty} \sum_{k_2=0}^{n_3} \frac{\mathcal{E}_1 \mathcal{A}_4 \mathcal{X}_1 \mathcal{A}_5 \mathcal{F}_2 (\tilde{\alpha}_m)^{-\left(\frac{2\epsilon_o^2 + \beta_o}{2\beta_o} + 1\right)} (k_2)^{\frac{2k_1 + 2\tilde{\alpha}_m \mu_n - \tilde{\alpha}_m}{2\tilde{\alpha}_m}}}{(2\pi)^{\frac{1}{2}(k_2 - 1) + \frac{1}{2}(\tilde{\alpha}_m - 1)} (\mathcal{A}_3 + \mathcal{E}_2)^{\frac{k_1 + \tilde{\alpha}_n \mu_n}{\tilde{\alpha}_m}}} \times G_{2\tilde{\alpha}_m + k_2, 3\tilde{\alpha}_m}^{2\tilde{\alpha}_m, \tilde{\alpha}_m + k_2} \left[\frac{(\mathcal{X}_2 \mathcal{F}_3)^{\tilde{\alpha}_m} (\tilde{\alpha}_m)^{-\tilde{\alpha}_m}}{(\mathcal{A}_3 + \mathcal{E}_2)^{k_2} k_2^{-k_2}} \middle| \begin{matrix} \Delta(\tilde{\alpha}_m, \psi), \Delta(k_2, 1 - \frac{k_1 + \tilde{\alpha}_m \mu_n}{\tilde{\alpha}_m}), \Delta(\tilde{\alpha}_m, 1) \\ \Delta(\tilde{\alpha}_m, 0), \Delta(\tilde{\alpha}_m, \psi), \Delta(\tilde{\alpha}_m, -\frac{\epsilon_o^2}{\beta_o}) \end{matrix} \right]. \tag{53}$$

This article has been accepted for publication in a future issue of this journal, but has not been fully edited. Content may change prior to final publication. Citation information: DOI 10.1109/ACCESS.2021.3078610, IEEE Access

$$\text{PNSC} = \sum_{n_1=0}^{j\tilde{\alpha}_m} \frac{\mathcal{A}_5\,\mathcal{E}_1\,\mathcal{A}_4\,\mathcal{F}_1\left(\frac{\tilde{\alpha}_n\mu_n+n_1}{\tilde{\alpha}_m}-1\right)!}{(\mathcal{A}_3+\mathcal{E}_2)^{\frac{\tilde{\alpha}_n\mu_n+n_1}{\tilde{\alpha}_m}}\,\tilde{\alpha}_m} - \sum_{n_2=0}^{\infty}\sum_{k_1=0}^{n_2}\sum_{n_3=0}^{\infty}\sum_{k_2=0}^{n_3} \frac{\mathcal{E}_1\,\mathcal{A}_4\,\mathcal{X}_1\,\mathcal{A}_5\,\mathcal{F}_2\,(\tilde{\alpha}_m)^{-\left(\frac{2\epsilon_o^2+\beta_o}{2\beta_o}+1\right)}(k_2)^{\frac{2k_1+2\tilde{\alpha}_m\mu_n-\tilde{\alpha}_m}{2\tilde{\alpha}_m}}}{(2\pi)^{\frac{1}{2}(k_2-1)+\frac{1}{2}(\tilde{\alpha}_m-1)}(\mathcal{A}_3+\mathcal{E}_2)^{\frac{k_1+\tilde{\alpha}_n\mu_n}{\tilde{\alpha}_m}}} \times G_{2\tilde{\alpha}_m+k_2,3\tilde{\alpha}_m}^{2\tilde{\alpha}_m,\tilde{\alpha}_m+k_2}\left[\frac{(\mathcal{X}_2\mathcal{F}_3)^{\tilde{\alpha}_m}\,(\tilde{\alpha}_m)^{-\tilde{\alpha}_m}}{(\mathcal{A}_3+\mathcal{E}_2)^{k_2}\,k_2^{-k_2}}\middle|\begin{matrix}\Delta(\tilde{\alpha}_m,\psi),\Delta(k_2,1-\frac{k_1+\tilde{\alpha}_m\mu_n}{\tilde{\alpha}_m}),\Delta(\tilde{\alpha}_m,1)\\ \Delta(\tilde{\alpha}_m,0),\Delta(\tilde{\alpha}_m,\psi),\Delta(\tilde{\alpha}_m,-\frac{\epsilon_o^2}{\beta_o})\end{matrix}\right]. \tag{55}$$

of curve is corroborated with the results obtained from MC simulations by generating 10^6 random samples in MATLAB. Various atmospheric turbulence conditions are assumed on the basis of Rytov variance. The weak, moderate, and strong turbulence conditions are specified by $\delta_R^2 < 1$, $\delta_R^2 \approx 1$, and $\delta_R^2 >> 1$, respectively [55, Eq. (2)]. The values of α_0, β_0, and η_0 for weak-to-strong atmospheric turbulence conditions are extracted from the best PDF fitting in [54], [56].

Figure 2 illustrates the ASC performance of the dual-hop system as a function of μ_{im} with $D = 3$ mm, $D = 13$ mm, and $D = 100$ mm. In this figure we consider strong

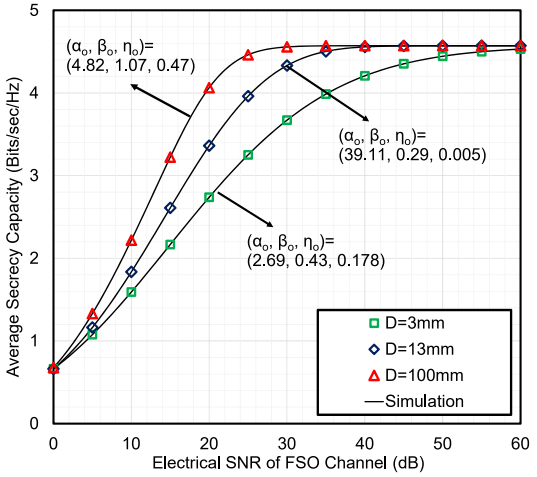

FIGURE 2: ASC versus μ_{im} for selected values of D under strong turbulence condition, and IM/DD detection where $\alpha_m = \alpha_n = 6$, $\mu_m = \mu_n = 5$, $\overline{\gamma}_m = 20$ dB, and $\overline{\gamma}_n = -20$ dB.

atmospheric turbulence condition i.e. $\delta_R^2 = 19.2$ for which we assume a Gaussian beam of $\lambda = 780$ nm propagating along a 1500 m horizontal path with a RI structure constant of 4.58×10^{-13} m$^{2/3}$ and $\rho_0 = 2.94$ mm. It is noted from the figure that ASC increases with the aperture averaging. Similar to Figs 4 and 3, it can be safely concluded that receiver with smaller aperture size ($D = 3$ mm) requires a higher SNR to ensure higher level of security compared to the aperture averaged receiver ($D = 13$ mm, 100 mm) since the irradiance fluctuations over an aperture are always averaged by an aperture averaged receiver that results in a lesser scintillation [57]. Moreover, a perfect similarity between MC and analytical results explore that expression of ASC in (32) is accurate.

Figure 3 depicts SOP versus the average SNR of the FSO link $\overline{\gamma}_{o_2}$ demonstrating the effects of various aperture sizes under moderate turbulence scenario for which we assume $\lambda = 780$ nm, $L = 1,225$ m, $C_n^2 = 2.1 \times 10^{-14}$ m$^{2/3}$, and the corresponding δ_R^2 and ρ_0 are 1.35 and 9.27 mm, respectively. We choose four aperture sizes i.e. $D = 3, 25, 60$, and 80 mm,

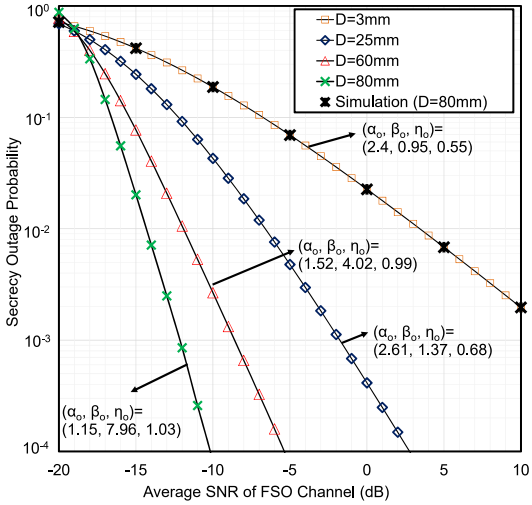

FIGURE 3: SOP versus $\overline{\gamma}_{o_2}$ for selected values of D under moderate turbulence condition, and IM/DD detection where $\alpha_m = \alpha_n = 6$, $\mu_m = \mu_n = 5$, $\overline{\gamma}_m = 20$ dB, and $\overline{\gamma}_n = -20$ dB.

where $D = 3$ mm acts like a point receiver since D is smaller than ρ_0 in this particular scenario. We can observe the SOP performance enhances with increasing D that in turns helps to minimize the transmit optical power. For example, a SOP of 10^{-4} is obtained at a SNR of 3 dB for $D = 25$ mm whereas same SOP can be obtained at -5 dB and -10 dB with $D = 60$ mm and $D = 80$ mm, respectively.

In Fig. 4, the SOP is plotted against μ_{hd} for spherical beam, to inspect the effects of aperture size on SOP performance under weak turbulence ($\delta_R^2 = 0.15$). For this analysis, we consider $\lambda = 780$ nm, $L = 1000$ m, and $C_n^2 = 7.2 * 10^{-15} m^{2/3}$ thereby corresponding ρ_0 is obtained

This article has been accepted for publication in a future issue of this journal, but has not been fully edited. Content may change prior to final publication. Citation information: DOI 10.1109/ACCESS.2021.3078610, IEEE Access

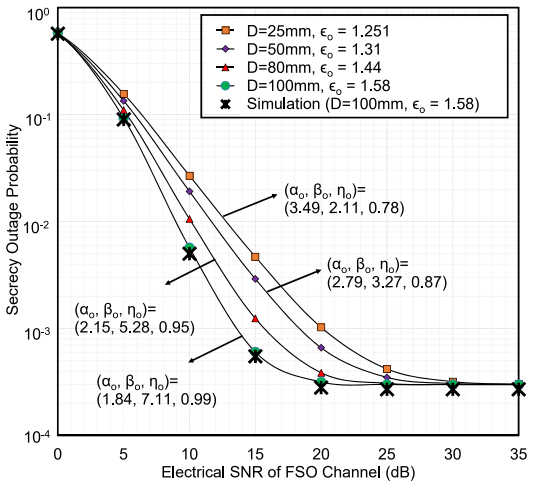

FIGURE 4: SOP versus μ_{hd} for selected values of D under weak turbulence condition while employing HD detection technique in presence of pointing error with $\alpha_m = \alpha_n = 3$, $\mu_m = \mu_n = 1$, $R_s = 0.5$, $\overline{\gamma}_m = 25$ dB, and $\overline{\gamma}_n = 0$ dB.

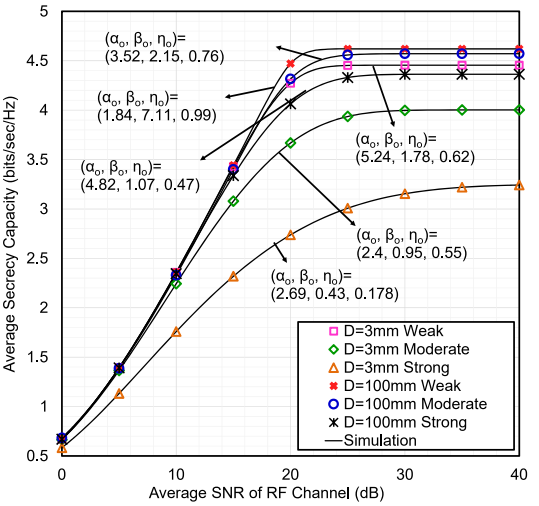

FIGURE 5: ASC versus $\overline{\gamma}_m$ for selected values of D under different turbulence conditions, and IM/DD detection where $\alpha_m = \alpha_n = 6$, $\mu_m = \mu_n = 5$, $\overline{\gamma}_{o_2} = 20$ dB, and $\overline{\gamma}_n = -20$ dB.

as 35 mm. Four aperture sizes are considered (i.e. 25, 50, 80, and 100 mm). It is clearly observed from the figure that the SOP performance improves considerably with an increase in D that is also confirmed in [6]. It is also noted with an increase in D, the diversity gain also increases. It is obvious, since in the case when the lens aperture at M is greater than the fading correlation length, the aperture averaging can be treated similar to the spatial diversity [55]. In each curve, it is also observed that the MC simulation exhibits a good agreement with the analytical results that clearly justifies the correctness of the derived result in (45).

The impacts of various turbulence severity on ASC, SOP, and PNSC are demonstrated in Figs. 5, 8, and 6, respectively, for a wide variety of aperture sizes (i.e. $D = 3$ mm, $D = 25$mm and 100 mm). Although an increased D is beneficial for security enhancement as noted in the previous figures, Figs. 5, 8, and 6 clearly reveal that higher the severity level of turbulence, lower the secrecy performance is. This indicates stronger turbulence affects the SNR at M more drastically rather than moderate and weak turbulence scenarios. Moreover, in Fig. 6, our simulation results are identical with the analytical results for $\overline{\gamma}_n = 0$ dB that ensures the preciseness of the derived PNSC expression in (55).

The ASC is depicted against $\overline{\gamma}_m$ in Fig. 7 to observe and demonstrate the impact of $\overline{\gamma}_n$ under moderate turbulence. It is observed that ASC decreases with $\overline{\gamma}_n$. This is expected as an increase in $\overline{\gamma}_n$ makes $S-E$ link stronger relative to the main channel and so the ASC deteriorates. Same observations were also made in [58] that confirms our results are correct.

Figures 8, and 9 describe the SOP performance against electrical SNR of FSO link to demonstrate the impact of the considered two detection techniques. It is noted that HD technique leads to a better secure outage performance relative to IM/DD technique. This is because the SNR is better at

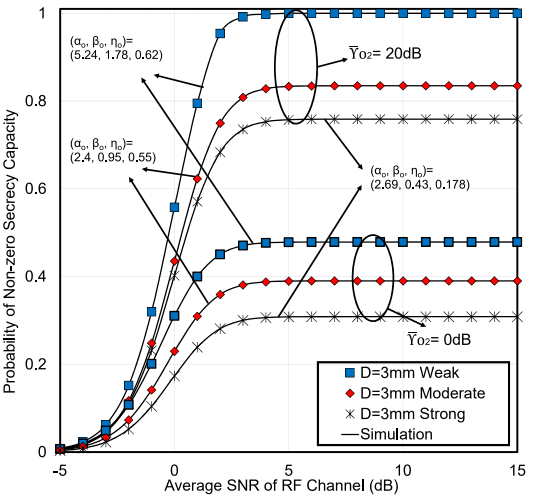

FIGURE 6: PNSC versus $\overline{\gamma}_m$ for different turbulence conditions of $D = 3$ mm, and IM/DD detection where $\alpha_m = \alpha_n = 5$, $\mu_m = 3$, $\mu_n = 2$, and $\overline{\gamma}_n = 0$ dB.

the receiver for the HD technique compared to the IM/DD technique as testified in [49].

A number of existing classical scenarios obtained as special cases of our proposed RF model are illustrated in Fig. 10. It is definitely observed that bsaed on the proposed $\alpha - \mu$ channel at the RF path, we can easily obtain Rayleigh, Gamma, Nakagami-m, Weibull, one sided Gaussian, Exponential etc. distributions as special cases (TABLE 1) simply via altering the values of the shape parameters (i.e. α and μ). This generic nature of the proposed RF-FSO scenario exhibits ample versatility over existing RF-FSO models that clearly boasts about the novelty and superiority of the proposed system.

In Figs. 11 and 12, the SOP and PNSC are plotted with

This article has been accepted for publication in a future issue of this journal, but has not been fully edited. Content may change prior to final publication. Citation information: DOI 10.1109/ACCESS.2021.3078610, IEEE Access

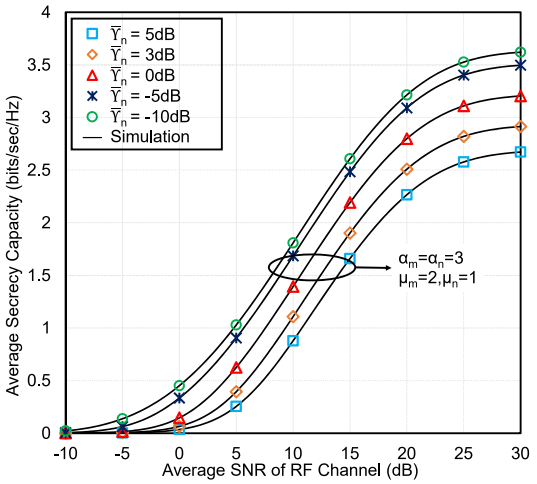

FIGURE 7: ASC versus $\overline{\gamma}_m$ for selected values of $\overline{\gamma}_n$ under moderate turbulence condition for the aperture size of $D = 3$ mm ($\alpha_o = 2.4$, $\beta_o = 0.95$, and $\eta_o = 0.55$), and IM/DD detection where $\alpha_m = \alpha_n = 3$, $\mu_m = 2$, $\mu_n = 1$, and $\overline{\gamma}_{o_2} = 20$ dB.

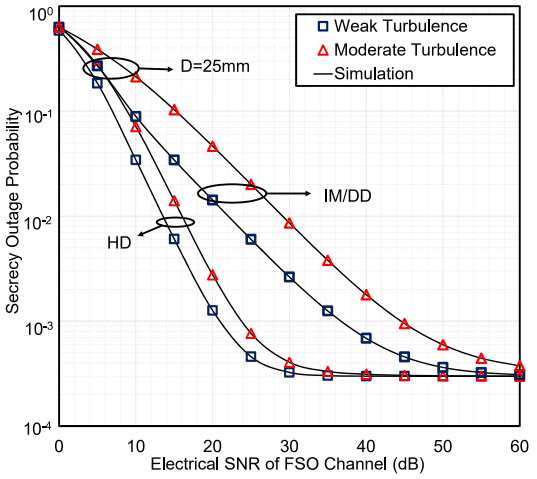

FIGURE 8: SOP versus μ_r for $D = 25$ mm under different turbulence conditions, and pointing error ($\epsilon_o = 1.251$) with $\alpha_m = \alpha_n = 3$, $\mu_m = \mu_n = 1$, $\overline{\gamma}_m = 25$ dB, and $\overline{\gamma}_n = 0$ dB.

respect to $\overline{\gamma}_{o_2}$ and $\overline{\gamma}_m$ to analyze the impacts of $\alpha_m, \alpha_n, \mu_m$, and μ_n with weak and moderate turbulent conditions, respectively. If we consider that $S - R$ and $S - E$ links undergo same amount of fading (i.e. $\alpha_m = \alpha_n$ and $\mu_m = \mu_n$) then the SOP will decrease and PNSC will increase significantly with the increased values of the fading parameters as described in [59]. Although smaller values of α_m and α_n represent severe non-linearity whereas smaller values of μ_m and μ_n indicates a sparse clustering for both $S - R$ and $S - E$ links. The $S-R$ link parameters impose more significant impacts on the secrecy performance rather than the $S - E$ link parameters.

Figures 13, and 14 illustrate the SOP and PNSC performances, respectively, as a function of electrical SNR of FSO channel with a view to observing the impacts of σ_s as well

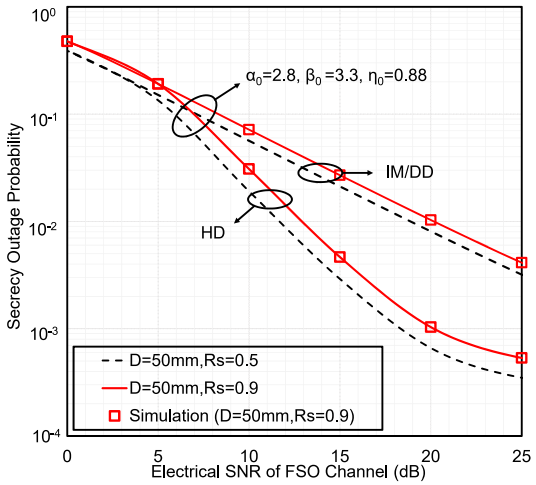

FIGURE 9: SOP versus μ_r for $D = 50$ mm under weak turbulence condition and pointing error ($\epsilon_o = 1.31$) with $\alpha_m = \alpha_n = 3$, $\mu_m = \mu_n = 1$, $\overline{\gamma}_m = 25$ dB, and $\overline{\gamma}_n = 0$ dB.

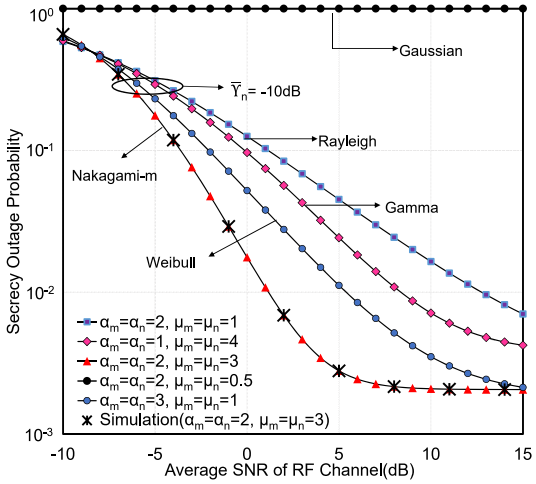

FIGURE 10: SOP versus $\overline{\gamma}_m$ for selected values of α and μ of both the RF channels under moderate turbulence condition for the aperture size of $D = 25$ mm ($\alpha_o = 2.61$, $\beta_o = 1.37$, and $\eta_o = 0.68$), and IM/DD detection where $\overline{\gamma}_{o_2} = 10$ dB.

as the pointing errors. It is obvious from the figures that with the increase of σ_s, the outage performance deteriorates. This occurs since an increase in σ_s signifies decrease in aperture size with an increased pointing error. The authors in [60] showed the same results that clearly justify our outcomes.

V. CONCLUSIONS

In this work, we examined the secrecy performance of a hybrid RF-FSO system over α-μ and unified EW mixed fading system with AF based variable gain relaying scheme under the attempt of an eavesdropper. Closed-form analytical expressions for the ASC, SOP, and PNSC were derived in terms of Meijer's G and Fox's H functions and MC simulations were performed to verify the derived expressions. The impacts of fading, pointing error, detection techniques,

This article has been accepted for publication in a future issue of this journal, but has not been fully edited. Content may change prior to final publication. Citation information: DOI 10.1109/ACCESS.2021.3078610, IEEE Access

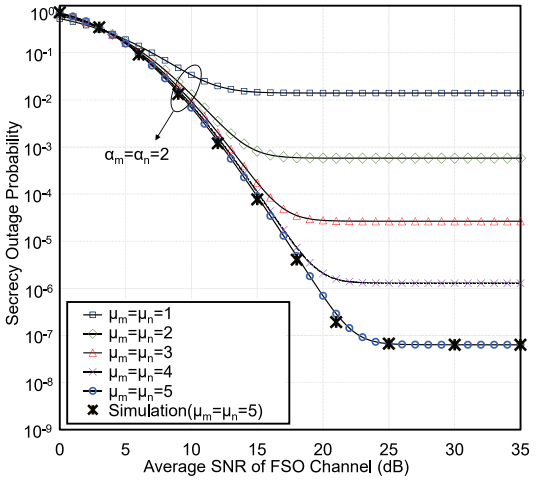

FIGURE 11: SOP versus $\overline{\gamma}_{o_2}$ for different values of μ of both the RF channels under weak turbulence condition for the aperture size of $D = 3$ mm ($\alpha_o = 5.24$, $\beta_o = 1.78$, and $\eta_o = 0.62$), and IM/DD detection where $\overline{\gamma}_m = 20$ dB and $\overline{\gamma}_n = 0$ dB.

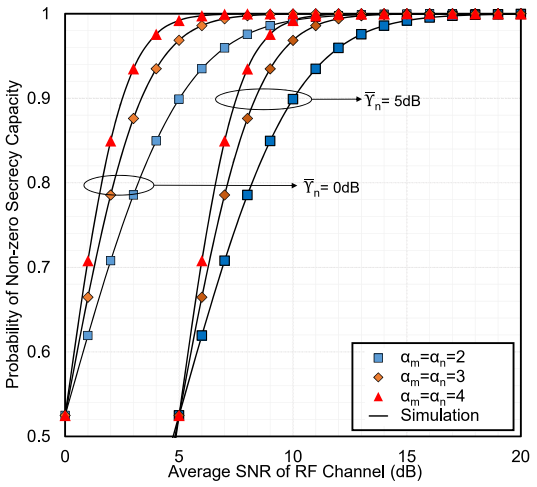

FIGURE 12: PNSC versus $\overline{\gamma}_m$ for different values of α and $\overline{\gamma}_n$ of both the RF channels under moderate turbulence condition for the aperture size of $D = 100$ mm ($\alpha_o = 3.52$, $\beta_o = 2.15$, and $\eta_o = 0.76$), and IM/DD detection where $\overline{\gamma}_{o_2} = 20$ dB, $\mu_m = 3$, and $\mu_n = 2$ dB.

and other system parameters of both RF and FSO hops were demonstrated and numerical results safely concluded that increasing lens aperture of the receiver is beneficial for secrecy capacity but as soon as the turbulence changes from weak-to-stronger conditions, the secrecy performance significantly deteriorates. Moreover, aperture averaging is more convenient for enhancing security of the mixed RF-FSO system in the case of HD technique than the IM/DD technique. Furthermore, the proposed model offers enormous versatility by exhibiting unification of secrecy performance over some well-known classical models as its special scenarios. Authors' next interest is to extend this work while

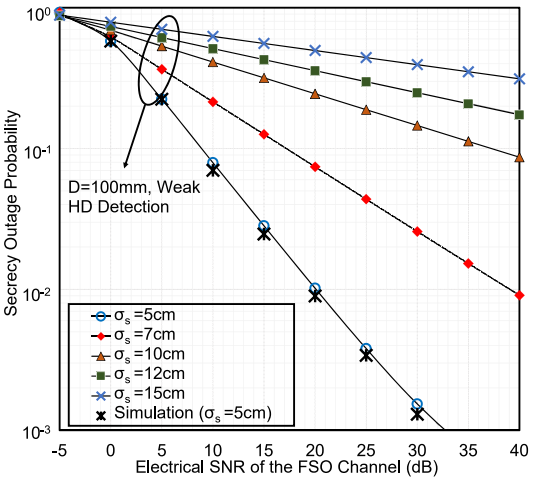

FIGURE 13: SOP versus μ_{hd} for different values of σ_s under weak turbulence condition for the aperture size of $D = 100$ mm ($\alpha_o = 1.84$, $\beta_o = 7.11$, and $\eta_o = 0.99$) and HD detection with $\overline{\gamma}_m = 25$ dB and $\overline{\gamma}_n = 0$ dB.

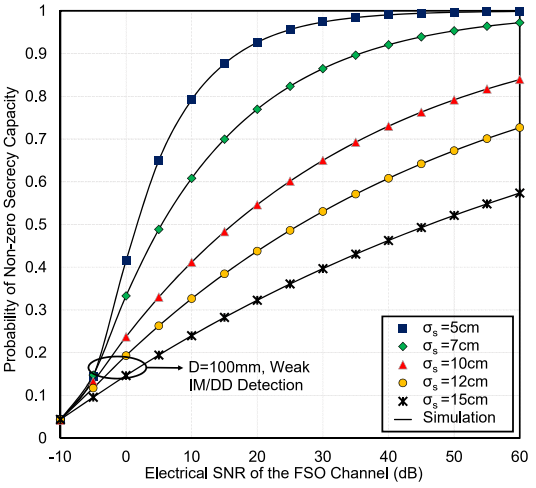

FIGURE 14: PNSC versus μ_{im} for different values of σ_s under weak turbulence condition for the aperture size of $D = 100$ mm ($\alpha_o = 1.84$, $\beta_o = 7.11$, and $\eta_o = 0.99$) and IM/DD detection with $\overline{\gamma}_m = 25$ dB and $\overline{\gamma}_n = 0$ dB.

modeling multi-hop networks and considering co-channel interference at the RF link.

APPENDIX.

We can express $\mathbb{E}[h_p^r]$ as [17]

$$\mathbb{E}[h_p^r] = \int {h_p}^r f_p(h_p) dh_p. \tag{56}$$

Substituting (16) into (56) and after some mathematical manipulations, we obtain

$$\begin{aligned}\mathbb{E}[h_p^r] &= \int_o^{A_o} {h_p}^r \frac{\epsilon_o^2}{{A_o}^{\epsilon_o^2}} h^{\epsilon_o^2 - 1} dh_p \\ &= \frac{\epsilon_o^2}{\epsilon_o^2 + r} {A_o}^r. \end{aligned} \tag{57}$$

Similarly, substituting (7) into (56), $\mathbb{E}[h_a^r]$ is expressed as

$$\begin{aligned}\mathbb{E}[h_a^r] &= \int {h_a}^r f_a(h_a) dh_a \\ &= \int {h_a}^r \frac{\alpha_o \beta_o}{\eta_o} \left(\frac{h_a}{\eta_o}\right)^{\beta_o - 1} exp\left[-\left(\frac{h_a}{\eta_o}\right)^{\beta_o}\right] \\ &\times \left\{1 - exp\left[-\left(\frac{h_a}{\eta_o}\right)^{\beta_o}\right]\right\}^{\alpha_o - 1} dh_a. \end{aligned} \quad (58)$$

Utilizing binomial theorem of [41, Eq. (1.110)], along with some basic manipulations, we express

$$\begin{aligned}\mathbb{E}[h_a^r] &= \frac{\alpha_o \beta_o}{\eta_o^{\beta_o}} \sum_{w=0}^{\infty} \binom{\alpha_o - 1}{w} (-1)^w \\ &\times \int_0^{\infty} {h_a}^{\beta_o + r - 1} exp\left[-(1+w)\left(\frac{h_a}{\eta_o}\right)^{\beta_o}\right] dh_a. \end{aligned} \quad (59)$$

Utilizing [41, Eq. (3.383.10)], eq. (59) is obtained as

$$\mathbb{E}[h_a^r] = \frac{\alpha_o}{\eta_o^{\beta_o}} \sum_{w=0}^{\infty} \binom{\alpha_o - 1}{w} \frac{(-1)^w}{\left\{\frac{1+w}{\eta_o}\right\}^{\beta_o + r}}. \quad (60)$$

REFERENCES

[1] M. A. Khalighi and M. Uysal, "Survey on free space optical communication: A communication theory perspective," IEEE communications surveys & tutorials, vol. 16, no. 4, pp. 2231–2258, 2014.

[2] D. Kedar and S. Arnon, "Urban optical wireless communication networks: the main challenges and possible solutions," IEEE Communications Magazine, vol. 42, no. 5, pp. S2–S7, 2004.

[3] S. Jiang, G. Yang, Y. Wei, M. Bi, Y. Lu, X. Zhou, M. Hu, and Q. Li, "Performance analysis of space-diversity free-space optical links over exponentiated Weibull channels," IEEE Photonics Technology Letters, vol. 27, no. 21, pp. 2250–2252, 2015.

[4] P. Wang, J. Qin, L. Guo, and Y. Yang, "BER performance of FSO limited by shot and thermal noise over exponentiated Weibull fading channels," IEEE Photonics Technology Letters, vol. 28, no. 3, pp. 252–255, 2015.

[5] M. Safari and M. Uysal, "Relay-assisted free-space optical communication," IEEE Transactions on Wireless Communications, vol. 7, no. 12, pp. 5441–5449, 2008.

[6] P. Wang, T. Cao, L. Guo, R. Wang, and Y. Yang, "Performance analysis of multihop parallel free-space optical systems over exponentiated Weibull fading channels," IEEE Photonics Journal, vol. 7, no. 1, pp. 1–17, 2015.

[7] L. B. Stotts, B. Stadler, and G. Lee, "Free space optical communications: coming of age," in Atmospheric Propagation V, vol. 6951. International Society for Optics and Photonics, 2008, p. 69510W.

[8] I. S. Ansari, F. Yilmaz, and M.-S. Alouini, "On the sum of squared η-μ random variates with application to the performance of wireless communication systems," in 2013 IEEE 77th Vehicular Technology Conference (VTC Spring), 2013, pp. 1–6.

[9] I. S. Ansari, M. M. Abdallah, M. Alouini, and K. A. Qaraqe, "Outage performance analysis of underlay cognitive RF and FSO wireless channels," in 2014 3rd International Workshop in Optical Wireless Communications (IWOW), 2014, pp. 6–10.

[10] I. S. Ansari, M. Alouini, and J. Cheng, "On the capacity of FSO links under Lognormal and Rician-Lognormal turbulences," in 2014 IEEE 80th Vehicular Technology Conference (VTC2014-Fall), 2014, pp. 1–6.

[11] I. S. Ansari and M. Alouini, "On the performance analysis of digital communications over Weibull-Gamma channels," in 2015 IEEE 81st Vehicular Technology Conference (VTC Spring), 2015, pp. 1–7.

[12] I. S. Ansari, M. M. Abdallah, M. Alouini, and K. A. Qaraqe, "Outage analysis of asymmetric RF-FSO systems," in 2016 IEEE 84th Vehicular Technology Conference (VTC-Fall), 2016, pp. 1–6.

[13] I. S. Ansari and M. Alouini, "Asymptotic ergodic capacity analysis of composite Lognormal shadowed channels," in 2015 IEEE 81st Vehicular Technology Conference (VTC Spring), 2015, pp. 1–5.

[14] F. Nadeem, V. Kvicera, M. S. Awan, E. Leitgeb, S. S. Muhammad, and G. Kandus, "Weather effects on hybrid FSO/RF communication link," IEEE journal on selected areas in communications, vol. 27, no. 9, pp. 1687–1697, 2009.

[15] N. I. Miridakis, M. Matthaiou, and G. K. Karagiannidis, "Multiuser relaying over mixed RF/FSO links," IEEE Transactions on Communications, vol. 62, no. 5, pp. 1634–1645, 2014.

[16] J. Zhang, L. Dai, Y. Zhang, and Z. Wang, "Unified performance analysis of mixed radio frequency/free-space optical dual-hop transmission systems," Journal of Lightwave Technology, vol. 33, no. 11, pp. 2286–2293, 2015.

[17] E. Zedini, I. S. Ansari, and M.-S. Alouini, "Performance analysis of mixed Nakagami-m and Gamma–Gamma dual-hop FSO transmission systems," IEEE Photonics Journal, vol. 7, no. 1, pp. 1–20, 2014.

[18] S. Anees and M. R. Bhatnagar, "Performance of an amplify-and-forward dual-hop asymmetric RF–FSO communication system," Journal of Optical Communications and Networking, vol. 7, no. 2, pp. 124–135, 2015.

[19] I. S. Ansari, F. Yilmaz, and M.-S. Alouini, "Impact of pointing errors on the performance of mixed RF/FSO dual-hop transmission systems," IEEE Wireless Communications Letters, vol. 2, no. 3, pp. 351–354, 2013.

[20] E. Soleimani-Nasab and M. Uysal, "Generalized performance analysis of mixed RF/FSO cooperative systems," IEEE Transactions on Wireless Communications, vol. 15, no. 1, pp. 714–727, 2015.

[21] L. Kong, W. Xu, L. Hanzo, H. Zhang, and C. Zhao, "Performance of a free-space-optical relay-assisted hybrid RF/FSO system in generalized m-distributed channels," IEEE Photonics Journal, vol. 7, no. 5, pp. 1–19, 2015.

[22] X. Yi, C. Shen, P. Yue, Y. Wang, and Q. Ao, "Performance of decode-and-forward mixed RF/FSO system over κ- μ shadowed and exponentiated Weibull fading," Optics Communications, vol. 439, pp. 103–111, 2019.

[23] Y. Zhang, X. Wang, S.-h. Zhao, J. Zhao, and B.-y. Deng, "On the performance of 2×2 DF relay mixed RF/FSO airborne system over exponentiated Weibull fading channel," Optics Communications, vol. 425, pp. 190–195, 2018.

[24] E. Erdogan, "Joint user and relay selection for relay-aided RF/FSO systems over exponentiated Weibull fading channels," Optics Communications, vol. 436, pp. 209–215, 2019.

[25] Z. Jing, Z. Shang-hong, Z. Wei-hu, and C. Ke-fan, "Performance analysis for mixed FSO/RF Nakagami-m and exponentiated Weibull dual-hop airborne systems," Optics Communications, vol. 392, pp. 294–299, 2017.

[26] Y. Wang, P. Wang, X. Liu, and T. Cao, "On the performance of dual-hop mixed RF/FSO wireless communication system in urban area over aggregated exponentiated Weibull fading channels with pointing errors," Optics Communications, vol. 410, pp. 609–616, 2018.

[27] E. Erdogan, N. Kabaoglu, I. Altunbas, and H. Yanikomeroglu, "On the error probability of cognitive RF-FSO relay networks over rayleigh/ew fading channels with primary-secondary interference," IEEE Photonics Journal, vol. 12, no. 1, pp. 1–13, 2019.

[28] E. Lee, J. Park, D. Han, and G. Yoon, "Performance analysis of the asymmetric dual-hop relay transmission with mixed RF/FSO links," IEEE Photonics Technology Letters, vol. 23, no. 21, pp. 1642–1644, 2011.

[29] L. B. Stotts, L. C. Andrews, P. C. Cherry, J. J. Foshee, P. J. Kolodzy, W. K. McIntire, M. Northcott, R. L. Phillips, H. A. Pike, B. Stadler et al., "Hybrid optical rf airborne communications," Proceedings of the IEEE, vol. 97, no. 6, pp. 1109–1127, 2009.

[30] I. S. Ansari, M. M. Abdallah, M. Alouini, and K. A. Qaraqe, "A performance study of two hop transmission in mixed underlay RF and FSO fading channels," in 2014 IEEE Wireless Communications and Networking Conference (WCNC), 2014, pp. 388–393.

[31] H. Lei, H. Luo, K.-H. Park, Z. Ren, G. Pan, and M.-S. Alouini, "Secrecy outage analysis of mixed RF-FSO systems with channel imperfection," IEEE Photonics Journal, vol. 10, no. 3, pp. 1–13, 2018.

[32] H. Lei, Z. Dai, K.-H. Park, W. Lei, G. Pan, and M.-S. Alouini, "Secrecy outage analysis of mixed RF-FSO downlink swipt systems," IEEE Transactions on Communications, vol. 66, no. 12, pp. 6384–6395, 2018.

[33] H. Lei, H. Luo, K.-H. Park, I. S. Ansari, W. Lei, G. Pan, and M.-S. Alouini, "On secure mixed RF-FSO systems with TAS and imperfect CSI," IEEE Transactions on Communications, 2020.

[34] L. Yang, T. Liu, J. Chen, and M.-S. Alouini, "Physical-layer security for mixed η-μ and $\mathcal{M}$-distribution dual-hop RF/FSO systems," IEEE Transactions on Vehicular Technology, vol. 67, no. 12, pp. 12 427–12 431, 2018.

[35] X. Pan, H. Ran, G. Pan, Y. Xie, and J. Zhang, "On secrecy analysis of DF based dual hop mixed RF-FSO systems," IEEE Access, vol. 7, pp. 66 725–66 730, 2019.

[36] A. H. Abd El-Malek, A. M. Salhab, S. A. Zummo, and M.-S. Alouini, "Security-reliability trade-off analysis for multiuser SIMO mixed RF/FSO relay networks with opportunistic user scheduling," IEEE Transactions on Wireless Communications, vol. 15, no. 9, pp. 5904–5918, 2016.

[37] S. Zvanovec, J. Perez, Z. Ghassemlooy, S. Rajbhandari, and J. Libich, "Route diversity analyses for free-space optical wireless links within turbulent scenarios," Optics express, vol. 21, no. 6, pp. 7641–7650, 2013.

[38] T. Tsiftsis, "Performance of heterodyne wireless optical communication systems over Gamma-Gamma atmospheric turbulence channels," Electronics Letters, vol. 44, no. 5, pp. 372–373, 2008.

[39] H. Lei, I. S. Ansari, G. Pan, B. Alomair, and M.-S. Alouini, "Secrecy capacity analysis over $\alpha - \mu$ fading channels," IEEE Communications Letters, vol. 21, no. 6, pp. 1445–1448, 2017.

[40] M. D. Yacoub, "The α-μ distribution: A physical fading model for the stacy distribution," IEEE Transactions on Vehicular Technology, vol. 56, no. 1, pp. 27–34, 2007.

[41] I. S. Gradshteyn and I. M. Ryzhik, Table of integrals, series, and products. Academic press, 2014.

[42] P. K. Sharma, A. Bansal, P. Garg, T. A. Tsiftsis, and R. Barrios, "Performance of fso links under exponentiated weibull turbulence fading with misalignment errors," in 2015 IEEE International Conference on Communications (ICC). IEEE, 2015, pp. 5110–5114.

[43] I. S. Ansari, F. Yilmaz, and M.-S. Alouini, "Performance analysis of free-space optical links over Málaga ($\mathcal{M}$) turbulence channels with pointing errors," IEEE Transactions on Wireless Communications, vol. 15, no. 1, pp. 91–102, 2015.

[44] P. K. Sharma, A. Bansal, P. Garg, T. Tsiftsis, and R. Barrios, "Relayed fso communication with aperture averaging receivers and misalignment errors," IET Communications, vol. 11, no. 1, pp. 45–52, 2017.

[45] L. C. Andrews and R. L. Phillips, "Laser beam propagation through random media." SPIE, 2005.

[46] A. P. Prudnikov, J. A. Bryčkov, and O. I. Maričev, Integrals and series. Vol. 3, More special functions. Gordon and Breach, 2003.

[47] M. O. Hasna and M.-S. Alouini, "A performance study of dual-hop transmissions with fixed gain relays," IEEE transactions on wireless communications, vol. 3, no. 6, pp. 1963–1968, 2004.

[48] K. O. Odeyemi and P. A. Owolawi, "Impact of non-zero boresight pointing errors on multiuser mixed RF/FSO system under best user selection scheme," Int. J. Microw. Opt. Technol, vol. 14, no. 3, pp. 210–222, 2019.

[49] S. H. Islam, A. Badrudduza, S. R. Islam, F. I. Shahid, I. S. Ansari, M. K. Kundu, S. K. Ghosh, M. B. Hossain, A. S. Hosen, and G. H. Cho, "On secrecy performance of mixed generalized Gamma and Málaga RF-FSO variable gain relaying channel," IEEE Access, 2020.

[50] M. D. Springer, "The algebra of random variables," Tech. Rep., 1979.

[51] P. Mittal and K. Gupta, "An integral involving generalized function of two variables," in Proceedings of the Indian academy of sciences-section A, vol. 75, no. 3. Springer, 1972, pp. 117–123.

[52] H. Lei, H. Zhang, I. S. Ansari, C. Gao, Y. Guo, G. Pan, and K. A. Qaraqe, "Performance analysis of physical layer security over generalized-k fading channels using a mixture Gamma distribution," IEEE Communications Letters, vol. 20, no. 2, pp. 408–411, 2015.

[53] G. Pan, C. Tang, X. Zhang, T. Li, Y. Weng, and Y. Chen, "Physical-layer security over non-small-scale fading channels," IEEE Transactions on Vehicular Technology, vol. 65, no. 3, pp. 1326–1339, 2015.

[54] R. Barrios and F. Dios, "Exponentiated Weibull model for the irradiance probability density function of a laser beam propagating through atmospheric turbulence," Optics & Laser Technology, vol. 45, pp. 13–20, 2013.

[55] M.-A. Khalighi, N. Schwartz, N. Aitamer, and S. Bourennane, "Fading reduction by aperture averaging and spatial diversity in optical wireless systems," IEEE/OSA Journal of Optical Communications and Networking, vol. 1, no. 6, pp. 580–593, 2009.

[56] R. Barrios and F. Dios, "Exponentiated Weibull distribution family under aperture averaging for gaussian beam waves," Optics express, vol. 20, no. 12, pp. 13 055–13 064, 2012.

[57] F. S. Vetelino, C. Young, L. Andrews, and J. Recolons, "Aperture averaging effects on the probability density of irradiance fluctuations in moderate-to-strong turbulence," Applied Optics, vol. 46, no. 11, pp. 2099–2108, 2007.

[58] M. J. Saber and A. Keshavarz, "On secrecy performance of mixed Nakagami-m and Málaga RF-FSO variable gain relaying system," in Electrical Engineering (ICEE), Iranian Conference on. IEEE, 2018, pp. 354–357.

[59] D. B. Da Costa and M. D. Yacoub, "Average channel capacity for generalized fading scenarios," IEEE Communications Letters, vol. 11, no. 12, pp. 949–951, 2007.

[60] Y. Wu, Y. Hao, H. Liu, L. Zhao, T. Jiang, D. Deng, and Z. Wei, "Performance improvement for wireless sensors networks by adopting hybrid subcarrier intensity modulation over exponentiated weibull turbulence channels," IEEE Access, vol. 8, pp. 118 612–118 622, 2020.

AUTHORS BIOGRAPHY

NAZMUL HASSAN JUEL is currently pursuing his Bachelor of Science (B.Sc) in Electronics & Telecommunication Engineering (ETE) from Rajshahi University of Engineering & Technology (RUET), Rajshahi, Bangladesh. His research interest includes physical layer security, cooperative relaying, FSO communication and non-orthogonal multiple access (NOMA).

A. S. M. BADRUDDUZA has received his Bachelor of Science (BSc) and Masters of Science (MSc) in Electrical & Electronic Engineering (EEE) from Rajshahi University of Engineering & Technology (RUET), Rajshahi, Bangladesh, in 2016 and 2019, respectively.

From 16 September 2016 to 22 July 2017 he was a Lecturer in the department of EEE at Bangladesh Army University of Engineering & Technology(BAUET), Natore, Rajshahi, Bangladesh. From 23 July 2017 to 29 June 2020 he was a lecturer in the Department of Electronics and Telecommunication Engineering (ETE) at RUET. He is now working as an assistant professor in the Department of ETE, RUET since 30 June 2020. He has been affiliated with IEEE since 2020 and is an active reviewer for several IEEE journals. His research interest includes physical layer security in multicast, cellular and cooperative networks, Free Space Optics (FSO), Underwater Optics (UWO), NOMA systems, etc.

Mr. Badrudduza has authored/co-authored 30+ international journals/conference publications. He was a recipient of two EEE Association Awards (Student of the Year Award) from RUET for his outstanding academic performances in the 1st and 4th-year examinations while pursuing his BSc engineering degree and two Best Paper Awards for two different research papers from IEEE Region 10 Symposium (TENSYMP2020), and IEEE 3rd International Conference on Telecommunication and Photonics (ICTP2019).

S. M. RIAZUL ISLAM (M'10) has been working as an assistant professor with the department of computer science and engineering at Sejong University, South Korea since March 2017. From 2014 to 2017, he worked at the wireless communications research center, Inha University, Korea as a post-doctoral fellow. In 2016-17, Dr. Islam was also affiliated with the Memorial University, Canada as a post-doctoral fellow. From 2005 to 2014, he was with the University of Dhaka, Bangladesh as an assistant professor and lecturer at the department of electrical and electronic engineering. In 2014, he worked at the Samsung R&D Institute Bangladesh as a chief engineer at the department of solution lab for advanced research. His research interests include wireless communications, internet of things, and applied artificial intelligence.

SHEIKH HABIBUL ISLAM is currently pursuing his Bachelor of Science (B.Sc) in Electrical & Electronic Engineering (EEE) degree from Rajshahi University of Engineering & Technology (RUET), Rajshahi, Bangladesh. His research interest includes FSO communication, physical layer security and NOMA system.

MILTON KUMAR KUNDU has received his BSc in Electrical & Electronic Engineering (EEE) from Rajshahi University of Engineering & Technology (RUET), Kajla, Rajshahi-6204, in 2016.

He has worked as the Lecturer in the department of EEE at North Bengal International University, Rajshahi, Bangladesh from 20 May, 2017 to 14 February, 2019. He is now working as the Lecturer in the Department of Electrical & Computer Engineering (ECE), RUET since 16 February, 2019. He is also the Advisor of IEEE RUET Industry Applications Society (IAS) Student Branch Chapter. His research interests are centered around the security aspects of cooperative and physical-layer networks and wireless multicasting.

Mr. M. K. Kundu has won several awards including the 2nd runner-up award in regional Mathematical Olympiad and EEE Association Award (Student of the Year Award) from RUET for his outstanding academic performances in the 3rd year examinations while pursuing BSc engineering degree. He has also won two Best Paper Awards for two different research papers from IEEE Region 10 Symposium (TENSYMP 2020), and IEEE 3rd International Conference on Telecommunication and Photonics (ICTP 2019).

IMRAN SHAFIQUE ANSARI (S'07–M'15) received the B.Sc. degree in Computer Engineering from King Fahd University of Petroleum and Minerals (KFUPM) in 2009 (with First Honors) and M.Sc. and PhD degrees from King Abdullah University of Science and Technology (KAUST) in 2010 and 2015, respectively. Currently, since August 2018, he is a Lecturer (Assistant Professor) with University of Glasgow, Glasgow, UK. Prior to this, from November 2017 to July 2018, he was a Lecturer (Assistant Professor) with Global College of Engineering and Technology (GCET) (affiliated with University of the West of England (UWE), Bristol, UK). From April 2015 to November 2017, he was a Postdoctoral Research Associate (PRA) with Texas AM University at Qatar (TAMUQ). From May 2009 through Aug. 2009, he was a visiting scholar with Michigan State University (MSU), East Lansing, MI, USA, and from Jun. 2010 through Aug. 2010, he was a research intern with Carleton University, Ottawa, ON, Canada.

He has been affiliated with IEEE and IET since 2007 and has served in various capacities. He is serving on the IEEE Nominations and Appointments (NA) Committee since 2020-2021 and IEEE Communication Society Young Professionals (ComSoc YP) Board since April 2016. He is part of the IEEE 5G Tech Focus Publications Editorial Board since Feb. 2017. He is serving as the Past-Chair of the IET Young Professionals Communities Committee (YPCC) from Oct. 2020-Sep. 2021. He has served on the IET Satellites Technical Network (TN) from Mar. 2016-Sep. 2020. He has served on the IET CC-EMEA (Communities Committee-Europe, Middle-East and Africa) for two complete terms from Oct. 2015-Sep. 2018 and Oct. 2010-Sep. 2013. He is an active reviewer for various IEEE Transactions and various other journals. He has served as a TPC for various IEEE conferences. He is a recipient of appreciation for an exemplary reviewer for IEEE Transaction on Communications (TCOM) in 2018 and 2016, a recipient of appreciation for an exemplary reviewer for IEEE Wireless Communications Letters (WCL) in 2017 and 2014, a recipient of TAMUQ ECEN Research Excellence Award 2016, 2017, a recipient of recognized reviewer certificate by Elsevier Optics Communications in 2015, a recipient of recognized reviewer certificate by OSA Publishing in 2014, a recipient of post-doctoral research award (PDRA) (first cycle) with Qatar national research foundation (QNRF) in 2014, a recipient of KAUST academic excellence award (AEA) in 2014, and a recipient of IEEE Richard E. Merwin student scholarship award in Jul. 2013.

Dr. Ansari has authored/co-authored 100+ journal and conference publications. He has co-organized the GRASNET'2016, 2017, 2018 workshops in conjunction with IEEE WCNC'2016, 2017 and IEEE Globecom 2018. His current research interests include free-space optics (FSO), underwater communications, physical layer secrecy issues, full duplex systems, and secure D2D applications for 5G+ systems, among others.

MD. MUNJURE MOWLA is now working as an Associate Professor in Electronics & Telecommunication Engineering (ETE) department of Rajshahi University of Engineering & Technology (RUET), Bangladesh. He has completed PhD degree in Wireless Communication Engineering from Edith Cowan University (ECU), Australia in 2018. During his PhD period, he achieved ECU merit top up scholarship (top 5% students in university). He was also awarded a competitive grant from Avaya Inc. Limited (previously known as Nortel Ltd). He is also experienced of writing proposal for NSF grants (US) and H2020 projects (EU) as an R&D Expert. He served as an active joint secretary in IEEE ICECTE 2019 and served other conferences as TPC member. He also attended IEEE conferences in Australia, Thailand, Japan, India, Bangladesh, and USA.

Dr Mowla worked as a professional Engineer in different telecommunication companies, i.e., ICX, Operator, and subcontractors from 2006 to 2010. He is also experienced with various Vendors equipment's, e.g., Huawei, ZTE, Ericsson, Samsung, Sungil, Korean Telecom, and Kathrein. He performed several technical visit in Australian telecommunication companies, i.e., Telstra and Vodafone. Mr. Mowla has published several international journals, transactions as well as conference papers and three books. He is a member of IEEE, ComSoc (IEEE), Institutions of Engineers, Bangladesh (IEB) and Bangladesh Electronics Society (BES). His research interest includes beyond 5G/6G Systems, Radio Resource Management, Machine Learning, Millimeter Wave, Software defined radio, D2D, Cloud RAN, Internet of Things, Ad hoc Networks, and Unmanned Aerial Networks. He also serves as a Reviewer of IEEE Transactions on Green Communication & Networking (TGCN), IEEE Transactions on Sustainable Computing (TSUSC), IEEE Access etc.

KYUNG-SUP KWAK ((Life Senior Member, IEEE) received the Ph.D. degree from the University of California. He was with Hughes Network Systems and the IBM Network Analysis Center, USA. He was with Inha University, South Korea, as a Professor. He was also the Dean of the Graduate School of Information Technology and Telecommunications and the Director of the UWB Wireless Communications Research Center. In 2008, he was an Inha Fellow Professor (IFP). He is currently an Inha Hanlim Fellow Professor and also a Professor with the School of Information and Communication Engineering, Inha University, South Korea. His research interests include UWB radio systems, wireless body area networks and u-health networks, and nano and molecular communications. In 2006, he was the President of the Korean Institute of Communication Sciences (KICS) and the Korea Institute of Intelligent Transport Systems (KITS) in 2009. He received the official commendations for achievements of UWB radio technology research and development from the Korean President in 2009.